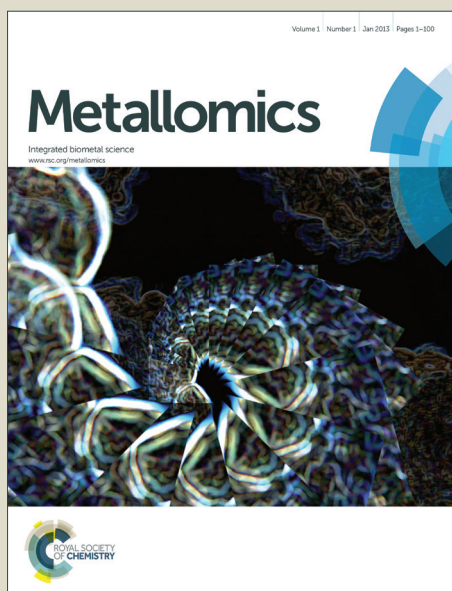


Metallomics

Accepted Manuscript



This is an *Accepted Manuscript*, which has been through the Royal Society of Chemistry peer review process and has been accepted for publication.

Accepted Manuscripts are published online shortly after acceptance, before technical editing, formatting and proof reading. Using this free service, authors can make their results available to the community, in citable form, before we publish the edited article. We will replace this *Accepted Manuscript* with the edited and formatted *Advance Article* as soon as it is available.

You can find more information about *Accepted Manuscripts* in the [Information for Authors](#).

Please note that technical editing may introduce minor changes to the text and/or graphics, which may alter content. The journal's standard [Terms & Conditions](#) and the [Ethical guidelines](#) still apply. In no event shall the Royal Society of Chemistry be held responsible for any errors or omissions in this *Accepted Manuscript* or any consequences arising from the use of any information it contains.

1
2
3
4
5
6
7
8
9
10
11
12
13
14
15
16
17
18
19
20
21
22
23
24
25
26
27
28
29
30
31
32
33
34
35
36
37
38
39
40
41
42
43
44
45
46
47
48
49
50
51
52
53
54
55
56
57
58
59
60

XAS and XFM Studies of Selenium and Copper Speciation and Distribution in the Kidneys of Selenite-Supplemented Rats

Claire M. Weekley,[†] Anu Shanu,[‡] Jade B. Aitken,[§] Stefan Vogt,[¶] Paul K. Witting,[‡] and Hugh H.
Harris^{†,*}

[†]*School of Chemistry and Physics, The University of Adelaide, SA 5005, Australia*

[‡]*The Discipline of Pathology, The University of Sydney, NSW 2006, Australia*

[§]*School of Chemistry, The University of Sydney, NSW 2006, Australia*

[¶]*X-Ray Science Division, Advanced Photon Source, Argonne National Laboratory, Lemont, IL
60439, USA*

*To whom correspondence should be addressed. Associate Professor Hugh Harris, *School of
Chemistry and Physics, The University of Adelaide, SA 5005, Australia* Phone: 61-08-83135060;
Facsimile: 61-8-83134358; Email: hugh.harris@adelaide.edu.au

Abstract

Dietary selenium has been implicated in the prevention of cancer and other diseases, but its safety and efficacy is dependent on the supplemented form and its metabolites. In this study, X-ray absorption spectroscopy (XAS) and X-ray fluorescence microscopy (XFM) have been used to investigate the speciation and distribution of Se and Cu *in vivo*. In kidneys isolated from rats fed a diet containing 5 ppm Se as selenite for 3 weeks, Se levels increased 5-fold. XFM revealed a strong correlation between the distribution of Se and the distribution of Cu in the kidney, a phenomenon that has previously been observed in cell culture (Weekley et al. in JBIC 2014, doi:10.1007/s00775-014-1113-x). However, X-ray absorption spectra suggest that most of the Se in the kidney is found as Se–Se species, rather than Cu-bound, and that most of the Cu is bound to S and N, presumably to amino acid residues in proteins. Furthermore, SOD1 expression did not change in response to the high Se diet. We cannot rule out the possibility of some Cu–Se bonding in the tissues, but our results suggest mechanisms other than the formation of Cu–Se species and SOD1 upregulation are responsible for the highly correlated distributions of Se and Cu in the kidneys of rats fed high selenite diets.

Abbreviations

DMSe, dimethylselenide; EXAFS, extended X-ray absorption fine structure; GPx, glutathione peroxidase; GSH, glutathione; GSSeH, glutathione selenenylsulfide; GSSeSG, selenodiglutathione; HSe⁻, hydrogen selenide; μ -XANES, microprobe-X-ray absorption near edge structure; MeSeCys, methylselenocysteine; OCT, Optimal Cutting Temperature (compound); ROS, reactive oxygen species; SeCys, selenocysteine; SelP, selenoprotein P; SeMet, selenomethionine; MeSeA, methylseleninic acid; TMS⁺, trimethylselenonium; TrxR, thioredoxin reductase; XANES, X-ray absorption near edge structure; XAS, X-ray absorption spectroscopy; XFM, X-ray fluorescence microscopy.

Introduction

Selenium is an essential element that is required for the assembly of selenoproteins. Selenoproteins have roles as antioxidants (glutathione peroxidases, GPx), in redox regulation (thioredoxin reductases, TrxR) and Se transport (selenoprotein P, SelP) amongst other functions, some of which remain to be elucidated.^{1,2} There is evidence that dietary supplementation with Se may be useful in the prevention of cancer³⁻⁷ and Se status has been linked to cardiovascular diseases and other health conditions.^{2,8,9} Yet the results of clinical trials have been mixed¹⁰⁻¹² and concerns about adverse health effects and the narrow therapeutic window of Se supplementation persist.^{13,14}

The biological activity of Se is dependent on its speciation: dietary Se compounds are each metabolised differently and act as pro-drugs for other metabolically active species.^{15,16} Inappropriate choice of Se supplement may be partly responsible for the failure of a recent clinical trial to protect against prostate cancer.¹⁷⁻¹⁹ An understanding of the metabolism, speciation and distribution of Se *in vivo* is paramount in selecting a safe and efficacious form(s) of Se to use in disease prevention.^{17,20}

Selenite is widely used in laboratory investigations of the effects of Se supplementation^{2,21-24} and is known to generate reactive oxygen species (ROS) and promote the oxidation of cellular thiols.^{4,25-29} Our current understanding of Se metabolism involves selenite reduction to hydrogen selenide (HSe^-) via selenodiglutathione (GSSeSG) and a glutathione selenenylsulfide (GSSeH). Selenite and GSSeSG are readily reduced by abundant glutathione (GSH), but they are also substrates for TrxR and both the thioredoxin and glutaredoxin systems reduced selenite to HSe^- .^{2,9,29-33} HSe^- is the purported common intermediate in the metabolism of dietary Se compounds. Methylation of HSe^- generates the Se excretion products dimethylselenide (DMSe) and trimethylselenonium (TMSe^+).^{11,12,34,35} Selenosugars are another excretory product.^{5,14,36,37} There is *in vitro* evidence that HSe^- is involved in the synthesis of monoselenophosphate, which is considered to be the source of Se for selenoprotein synthesis.^{16,38-41}

The speciation of Se *in vivo* has been explored in rat models, typically using hyphenated techniques that couple separation (chromatographic) to identification (mass spectrometric) techniques. The hyphenated techniques, typically high performance liquid chromatography-inductively coupled mass spectrometry (HPLC-ICP-MS), have been used to unequivocally identify some Se metabolites in cell lines, tissue homogenates and human urine, but many remain unidentified *in vivo*.^{10,18,19,42} In rats fed a Se-adequate diet Shiobara *et al.* found that the

1
2 kidneys (compared to the brain, liver and testes) accumulated the most Se with the concentration
3 peaking at 1.5 ppm.^{5,20,43} An early study investigated the relative amounts of selenomethionine
4 (SeMet) and selenocysteine (SeCys) in tissues and fluids of rats fed ⁷⁵Se-labelled selenite or
5 SeMet at approximately 5 ppm/day for 7 weeks. The experiment was limited to the identification
6 of SeMet and SeCys and the association of Se with GPx, haemoglobin and cell signaling G-
7 proteins.^{3,44} More extensive studies of the excretory metabolites generated by acute doses of
8 selenite, SeMet, methylselenocysteine (MeSeCys) and methylseleninic acid (MeSeA) have been
9 conducted by labeling the compounds with stable Se isotopes. For example, Suzuki *et al.*^{35,45}
10 documented the relative extent to which each of the compounds were available and converted to
11 selenosugar, GPx, SeIP and TMS⁺ metabolites, notably selenite did not reach the organs in its
12 intact form. The coupling of chromatography and mass spectrometry have also been used to
13 study the metabolism of Se compounds, including selenite, in rat hepatocytes⁴⁶⁻⁴⁸ and in human
14 cancer cells.⁴⁹

15
16
17
18
19
20
21
22
23
24
25
26
27
28
29
30
31
32
33
34
35
36
37
38
39
40
41
42
43
44
45
46
47
48
49
50
51
52
53
54
55
56
57
58
59
60
The combination of X-ray absorption spectroscopy (XAS) and X-ray fluorescence
microscopy (XFM) offers an alternative for determining the speciation and distribution of Se *in vivo*
and provides information that complements the information available from hyphenated
techniques. XAS can be used to determine the speciation of major and minor, but not trace, Se
metabolites *in vivo* with minimal sample preparation – as opposed to the digestion and extraction
of samples required by the hyphenated techniques that risk loss or (*ex vivo*) chemical alteration
of some species.¹ XFM also involves minimal sample preparation and is capable of mapping
elemental distributions of elements heavier than Si in tissue sections. The advantage of XAS and
XFM techniques over the hyphenated techniques is that information about elemental
distributions is retained in intact samples. We have previously used XAS and XFM in
combination to study Se speciation and distribution in human cancer cells supplemented with
SeMet or MeSeCys.^{3,5-7} XAS has been applied to the determination of Se speciation in trout
hepatocytes.⁸ XFM has been used to study the distribution of Se in the kidneys of rats subjected
to experimental myoglobinuria,¹⁰ in the sperm of mice¹³ and the kidneys of mice and naked mole
rats.¹⁵

Herein we describe the first combined application of XAS and XFM to the investigation of
Se speciation and distribution *in vivo*. The diets of rats were supplemented with up to 5 ppm Se
as selenite, leading to an increase in Se concentration sufficient for analysis by XAS and XFM.
We found that Se and Cu were colocalised in the kidney, but we found no evidence for the
formation of Cu–Se bonds.

Experimental

Se supplementation

Male Sprague-Dawley rats (80 – 100 g) were from the Animal Resources Centre (Perth, Australia). Animals were acclimated for 2 weeks, randomly assigned to groups, and provided normal chow or commercial sodium selenite supplemented diets *ad libitum*: diets prepared by Glen Forrest Specialty Feed (Perth, Western Australia) contained 1 ppm and 5ppm Se as selenite. Normal chow contained ~ 0.3 ppm Se of unknown chemical form, thus the Se-supplemented diets contained a total of 1.3 ppm or 5.3 ppm Se, of which 1 ppm and 5 ppm Se, respectively, was present as selenite. For simplicity the diets will be referred to as control (no added Se), 1 ppm Se (1 ppm Se added as selenite) and 5 ppm Se (5 ppm Se added as selenite) diets. After 3 weeks of diet, animal weights among the groups were not different: normal chow 230 ± 8 g ($n = 4$); 1 ppm Se diet 227 ± 8 g ($n = 4$), and 5 ppm Se diet 217 ± 8 g ($n = 4$). Studies were conducted according to Local Ethics guidelines that adhered to NIH Guidelines for the Care and Use of Laboratory Animals.

Harvest of kidneys

Animals were anaesthetised with isoflurane, followed by intraperitoneal injection of ketamine (50 mg/kg weight) and xylazine (10 mg/kg weight). The kidneys were harvested, the left kidney was sectioned, and the ventral portion was immersed in Tissue-Tek Optimal Cutting Temperature compound (OCT, ProSciTech, QLD, Australia) and stored at -80°C for preparation of frozen sections. The remaining sample was stored in 4% v/v formalin for histological analysis. The isolated right kidney was snap frozen in liquid nitrogen and stored at -80°C for subsequent molecular/biochemical analyses.

Preparation of tissue homogenate

Where required, intact frozen kidneys were thawed, diced, snap frozen in liquid nitrogen, pulverised to a fine powder and homogenised for use in gene response studies, as described previously¹⁷.

Tissue gene response

Total RNA was extracted from renal homogenates with a kit (GeneElute; Sigma Aldrich, Sydney, Australia) and cDNA was constructed using BioScript Reverse Transcriptase (Bio- line,

1
2
3
4
5
6
7
8
9
10
11
12
13
14
15
16
17
18
19
20
21
22
23
24
25
26
27
28
29
30
31
32
33
34
35
36
37
38
39
40
41
42
43
44
45
46
47
48
49
50
51
52
53
54
55
56
57
58
59
60

Sydney, Australia) using a PCR-MasterCycler (Eppendorf, Sydney, Australia).¹⁷ Gene expression was determined by q-PCR, quantified by the comparative Ct method, normalized against β -actin, and expressed as fold-change relative to the control using the following primer sequences: GPx1, forward 5'-TGAGAAGTGCGAGGTGAATG-3', reverse 5'-AACACCGTCTGGACCTACCA-3'; SOD1, forward 5'-CCACTGCAGGACCTCATTTT-3', reverse 5'-TCTTCATTTCCACCTTTGCC-3'.

Immunohistochemistry

Thin sections (5 μ m) were cut ($n = 1$ for each treatment group) and mounted onto SuperFrost Plus slides for staining using a Dako Auto-immunostainer. Sections were de-paraffinized, blocked with 3% v/v albumin in TBS-T and 5% v/v goat serum, then incubated with the appropriate primary antibody (dilution 1:200 v/v, 60 min). All sections were washed and incubated with a biotin-conjugated secondary antibody (1:250 v/v, 30 min, Vectastain ABC). Sections were washed, incubated with streptavidin-conjugated HRP (1:250v/v, 30 min, Vectastain ABC) and visualised with DAB (DAKO, Sydney Australia) after counterstaining with Mayer's haematoxylin and mounting using DPX solution (DAKO). Images were captured with an Olympus Microscope using a digital camera (DP Controller; v2.2.1.227) and converted to TIFF for handling with MS PowerPoint (2008, v7).

ICP-MS

Whole kidneys were freeze-dried before undergoing microwave assisted nitric acid digestion, following a modified version of US EPA Method 3052. NIST SRM 1577b was also freeze-dried and digested under the same protocol. Approximately 0.1 mL of each of the digests was taken to determine the concentration of Cu, Zn and Se by inductively-coupled plasma mass spectrometry (ICP-MS) (Agilent 7700).

X-ray fluorescence microscopy

Kidneys were cryo-sectioned (10 μ m and 30 μ m), mounted on to 5 mm \times 5 mm \times 500 \times nm silicon nitride windows (Silson, England) and freeze-dried as described elsewhere.²¹ XRF elemental distribution maps were collected on beamline 2-ID-E at the Advanced Photon Source (APS), Argonne National Laboratory, Illinois, USA and on the X-ray fluorescence microprobe (XFM) beamline at the Australian Synchrotron, Victoria, Australia.

At the APS the beam was tuned to an incident energy of 13 keV using a beam splitting Si(220) monochromator and was focused to a diameter of 0.6 μ m using a "high-flux" zone plate.

1
2
3
4
5
6
7
8
9
10
11
12
13
14
15
16
17
18
19
20
21
22
23
24
25
26
27
28
29
30
31
32
33
34
35
36
37
38
39
40
41
42
43
44
45
46
47
48
49
50
51
52
53
54
55
56
57
58
59
60

A single silicon drift energy dispersive detector (Vortex EX, SII Nanotechnology, Northridge, CA), at 90° to the incident beam, was used to collect the fluorescence signal. The fluorescence signal was collected from the tissue sections (10 μm thickness) under a He atmosphere in “fly scan” mode with a 40 ms dwell time and 6.5 μm ‘steps.’ Smaller regions were selected for higher resolution scans at 0.5 s dwell time and 1 μm step size.

For the smaller sections, the integrated fluorescence spectra were extracted from the images and fit with modified Gaussians to determine the average elemental content (in $\mu\text{g cm}^{-2}$) and quantification was performed by comparison to the corresponding measurements on thin-film standards NBS-1832 and NBS-1833 (National Bureau of Standards, Gaithersburg, MD). The average elemental content (in $\mu\text{g cm}^{-2}$) of the fly scans was extracted from per pixel fits of the fluorescence images. Analysis was performed using MAPS software.²⁵

At the Australian Synchrotron, the beam was tuned to an incident energy of 15.75 keV using a Si(220) monochromator and focused to a spot size of 2 μm using Kirkpatrick-Baez mirrors. A 384-element silicon array detector (Maia 384, Brookhaven National Laboratory, Upton, NY and CSIRO, Clayton, Victoria³⁰) in 180° backscatter geometry was used to collect the fluorescence signal. The fluorescence signal was collected from tissue sections (30 μm thick) with a 4 ms dwell time and 2 μm ‘steps.’ A small region was selected for Se XANES imaging. The beam was focused to a 4 μm spot size and images were collected with an 8 ms dwell and 4 μm steps. Images were collected across an energy range of 12500 to 12900 eV at the following intervals: pre-edge region 12500 – 12640 eV (10 eV steps), edge region 12640 – 12655 (1 eV steps), 12655 – 12675 (0.5 eV steps), 12675 – 12700 (1 eV steps) and post-edge region 12700 – 12900 (20 eV steps).

The fit to a representative fluorescence spectrum was used to generate a dynamic analysis matrix that was used to project the images. Quantification was performed by corresponding measurements and analysis on a Pt standard. XANES spectra were extracted from regions of interest in the XANES stack images and calibrated to the first peak of the first derivative of a Se foil standard (12658 eV). Analysis was performed using GeoPIXE and EXAFSPAK (as described in Section 8.4.8) software.

X-ray absorption spectroscopy

Selenium K-edge X-ray absorption spectra of the rat tissues were recorded at the Stanford Synchrotron Radiation Lightsource (SSRL), Stanford, CA on beamline 9-3. The X-ray beam was monochromated by diffraction from a pair of Si(220) crystals. Harmonic rejection was achieved

1
2
3
4
5
6
7
8
9
10
11
12
13
14
15
16
17
18
19
20
21
22
23
24
25
26
27
28
29
30
31
32
33
34
35
36
37
38
39
40
41
42
43
44
45
46
47
48
49
50
51
52
53
54
55
56
57
58
59
60

by setting the cutoff energy of a Rh-coated mirror to 15 keV. Samples were cooled to ~10 K in a flowing He cryostat. Spectra from frozen whole tissue samples were recorded in fluorescence mode on a 30-element or 100-element Ge detector array (Canberra) at 90° to the incident beam. A 3 absorption path-length As filter and Soller slits were optimally positioned between the sample and the detector to reduce the elastic scatter peak.

Se K-edge EXAFS spectra were collected at the following energy ranges: pre-edge region 12435–12635 eV (10 eV steps); XANES region 12635–12685 eV (0.25 eV steps); and EXAFS region 12685–13443 eV (0.05 Å⁻¹ steps in *k*-space to 14.2 Å⁻¹). A Se foil standard (hexagonal allotrope of Se) was used to calibrate the energy scale to the first peak of the first derivative of the Se edge (12658 eV). Cu K-edge EXAFS spectra were collected at the following energy ranges: pre-edge region 8750–8960 eV (10 eV steps); XANES region 8960–9010 eV (0.35 eV steps); EXAFS region 9010–9768 eV (0.05 Å⁻¹ steps in *k*-space to 12.8 Å⁻¹). An elemental Cu foil standard was used to calibrate the energy scale to the first peak of the first derivative of the Cu edge (8979 eV). Multiple spectra were collected from each sample in order to produce average spectra and increase the signal-to-noise ratio. Sequential spectra from the same samples were compared to ensure that there was no photoreduction of the redox-active Se and Cu centres during repeat scans.

Calibration, averaging and background subtraction of XANES and EXAFS spectra was performed using the EXAFSPAK software package (G. N. George, SSRL, <http://www-ssrl.slac.stanford.edu/exafspak.html>). Linear combination fits of XANES spectra were performed over the region 12600–12750 eV for Se K-edge spectra and over the region 8950–9050 eV for Cu K-edge spectra, also using EXAFSPAK. Some spectra of model Se and Cu compounds for comparison to experimental spectra were provided by G. N. George (University of Saskatchewan) and Enzo Lombi (University of South Australia).

Results

Cu and Se are colocalised in the kidney

XFM reveals that the distributions of Se and Cu in the 5 ppm Se kidney section are highly correlated and distinct from the distributions of other endogenous elements (Figure 1). In the 1 ppm Se and control kidney sections, Se is indistinguishable from the background and Cu is ubiquitously distributed across the tissues (Figure 1b and c). Both Cu and Se are highly

1
2 concentrated in some regions of the kidney isolated from the 5 ppm Se group and absent in
3 others, whereas other endogenous elements (S, K, Fe, Zn) are more ubiquitously distributed
4 across the tissues (Figure 1c). No other elements (*e.g.* Mn or Ni) demonstrated distributions
5 similar to those of Se or Cu. A thicker section from the same kidney taken from an animal
6 supplemented with 5 ppm Se (Figure 2) shows the same Cu and Se colocalisation observed in
7 Figure 1c, where Se and Cu appear to be concentrated in the renal cortex.
8
9
10
11
12

13
14 An overlay of the Se and Cu maps of the kidney section from the animal supplemented with
15 5 ppm Se confirms the almost exact coincidence of the two elements that is independent of K
16 distribution that maps the tissue structure (Figures 3 and S1). At the smaller scale shown in
17 Figure 3, it is apparent that the regions of high Se and Cu observed in Figure 1c are composed of
18 thousands of groups of Cu and Se that are on the order of a few micrometers in size. Linear
19 regression of the Cu concentration against the Se concentration at each position (~ 14000 pixels)
20 in the small region shown in Figure 3 gives a slope of 1.036 ± 0.004 and an R^2 value of 0.84
21 (Figure 4), which confirms the strong correlation found by visual inspection.
22
23
24
25
26
27
28

29 *Se levels are increased by 5 ppm Se (as selenite) supplementation*

30
31 In addition to the colocalisation of Se and Cu, XFM revealed large increases in the
32 concentrations of the two elements of interest in the 5 ppm kidney section relative to the control
33 and 1 ppm kidney sections (Table 1). To verify this observation whole kidney tissues were
34 analysed for Se, Cu and Zn concentrations by ICP-MS. Rats fed the 5 ppm Se diet experienced a
35 10-fold increase in Se concentration in the kidneys compared to the Se adequate (control) diet
36 (Table 1). In the kidney of a rat fed the 1 ppm Se diet, Se concentrations remained unchanged
37 relative to the control diet. By contrast, the concentrations of Zn varied widely within and across
38 all three diets.
39
40
41
42
43
44
45
46

47 ICP-MS analysis showed no difference in the concentration of Cu in the bulk kidney tissues
48 of rats fed the two different Se-supplemented diets. Conversely, XFM analysis showed a 7-fold
49 increase in Cu concentration in the kidney section from the animal fed 5 ppm Se in the diet
50 compared to the control kidney section. The inconsistency may be the result of biological
51 variation between tissues or may indicate that the localisation of Cu observed in Figure 1c may
52 be due to a redistribution of Cu rather than an overall increase in kidney Cu concentration.
53
54
55
56
57
58

59 It should be noted that absolute elemental concentrations determined by XFM (Table 1)
60 differ significantly from those determined by ICP-MS (Table 2) because: the concentrations
determined by XFM were converted from $\mu\text{g cm}^{-2}$ to ppm with the assumptions that (a) the

1
2 sections were of uniform thickness and (b) had a density of 1.06 g cm^{-3} ;³⁴ and the kidney section
3 is not necessarily representative of the bulk tissue that was digested for ICP-MS analysis.
4 Nevertheless, a large increase in Se concentration in 5 ppm Se kidneys versus control kidneys
5 was indicated by both ICP-MS and XFM analysis.
6
7
8

9
10 *XAS spectra reveal Se–Se bonding, but not Se–Cu bonding, in 5 ppm Se kidney tissues*
11

12
13 The colocalisation of Se and Cu in the 5 ppm Se kidney could conceivably be due to the
14 formation of a Cu–Se moiety. The possibility of Cu–Se bonding was investigated by the
15 collection of Se and Cu K-edge XAS spectra from whole kidney tissues. XANES spectra provide
16 information on the oxidation state and chemical environment of the absorbing atom, unlike
17 analysis of EXAFS spectra, which allow the determination of bond lengths between the
18 absorbing atom and its neighbours. Se K-edge XANES spectra were collected from control, 1
19 ppm and 5 ppm Se kidney tissues: Se and Cu K-edge EXAFS spectra were collected from 5 ppm
20 Se kidney tissues. The concentrations of Se and Cu in the kidneys of control animals were too
21 long for collection of EXAFS spectra.
22
23
24
25
26
27
28
29

30 *XANES spectra*
31

32
33 A collection of Se model compound XANES spectra is shown in Figure 5 and includes XANES
34 spectra collected from kidneys of rats fed control, 1 ppm Se and 5 ppm Se diets. The Se model
35 compound library encompasses a broad range of Se coordination environments. The position of
36 the first peak of Se compound spectra changes with oxidation state, with more oxidised species
37 absorbing at higher energies, such that the different bonding environments have absorption edges
38 in order of energy: Se–Se bonds < Se–S bonds < Se–R bonds < Se–O bonds. Notably, the spectra
39 of the rat kidneys do not look like any single Se model compound, but the positions of their first
40 peaks lie between Se–Se and Se–S models (Figure 5).
41
42
43
44
45
46
47

48
49 From a set of model compounds encompassing likely coordination environments of Se in
50 biology, a linear combination of elemental Se (Se–Se–Se), CuSe, GPx (a model of SeCys in
51 selenoproteins) and GSSeSG (S–Se–S) produced the best fits to the Se K-edge XANES spectra
52 (Table 3). Corresponding tissue spectra from the control and animal receiving 1 ppm Se in the
53 diet are distinguished from the kidney section from animal fed 5 ppm Se in the diet by the lack
54 of elemental Se and greater proportions of S–Se–S species and GPx fit to the XANES spectra.
55 The XANES fits to spectra of the kidney section from animal fed 5 ppm Se in the diet contain
56 substantial proportions of elemental Se, which is expected from the similar energies of the first
57 peaks of these spectra to the peak of elemental Se.
58
59
60

1
2
3
4
5
6
7
8
9
10
11
12
13
14
15
16
17
18
19
20
21
22
23
24
25
26
27
28
29
30
31
32
33
34
35
36
37
38
39
40
41
42
43
44
45
46
47
48
49
50
51
52
53
54
55
56
57
58
59
60

Notably, CuSe constitutes a major proportion of all fitted XANES spectra and a majority of the 5 ppm spectra. This is a spurious result given the low Se concentrations and the lack of Se and Cu colocalisation in the kidney sections from control or animal receiving 1 ppm Se in the diet. Yet removal of CuSe from the fits and/or its replacement with HSe^- (similar peak position to CuSe) substantially worsened the fits. Despite our efforts to collect a broad range of model compounds, the very large proportions of CuSe, even in the control tissue, suggest that the presence of CuSe is compensating for an unknown missing component.

The speciation of Se in a small region where it was highly concentrated and colocalised with Cu was studied in detail (Figure 6). Microprobe-XANES spectra were extracted from XFM images of a small area ($330 \mu\text{m} \times 150 \mu\text{m}$) of the kidney section from animal fed 5 ppm Se in the diet collected at a number of energies across the Se absorption edge. These spectra were unlike the bulk kidney XANES spectra. They were also unlike the μ -XANES spectra that we have previously collected from regions of high Se concentration in human lung cancer cells treated with $5 \mu\text{M}$ selenite (also shown in Figure 6).⁵ The energy of the first peak of the μ -XANES is suggestive of a R–Se–R species. However, the same model compounds that were considered in the fitting of the bulk kidney spectra (elemental selenium, CuSe, CysSeH, CysSeSeCys, GPx and GSSeSG) failed to give a good linear combination fit to the kidney section μ -XANES (Figure S3 and Table S1). The stark difference in speciation between the kidney section μ -XANES and whole kidney XANES spectra (Figure 8) may be due to the small area of tissue that was examined, which may not be representative of the remainder of the tissue. Furthermore the preparation of the kidney sections, while minimal, was different to that of the bulk tissue. The sections were imaged as a freeze-dried, dehydrated section, whereas the whole organs were analysed as frozen, hydrated tissue.

Cu K-edge XANES spectra were collected from the kidney section from animals fed 5 ppm Se in the diet with a focus on the renal cortex and medulla. Visual comparison of these spectra to a spectrum of A549 human lung cancer cells treated with $5 \mu\text{M}$ selenite, reveals that there is a different Cu coordination environment in the cells and tissues (Figure 7a), despite both systems exhibiting a colocalisation of Cu and Se after selenite treatment. Additional comparisons of the tissue spectra to Cu model compounds of Cu–Se, Cu–S and Cu–N bonding and Cu proteins are made in Figure 7. None of the model compound spectra closely match the tissue spectra, but the Cu(II)-auracyanin a (Figure 7f) and Cu-metallothionein (Figure 7j) spectra share some broad similarities with the tissue spectra, particularly at the absorption edge. The similarities between the renal cortex and medulla spectra and the spectra of the Cu(II)-auracyanin a, which contains both Cu–S and Cu–N bonds³⁸ suggests that the Cu is likely bound to histidine, methionine and

1
2
3
4
5
6
7
8
9
10
11
12
13
14
15
16
17
18
19
20
21
22
23
24
25
26
27
28
29
30
31
32
33
34
35
36
37
38
39
40
41
42
43
44
45
46
47
48
49
50
51
52
53
54
55
56
57
58
59
60

cysteine groups in proteins. CuSe and various SOD spectra appear dissimilar to the tissue spectra, reinforcing the suspect fitting of CuSe to the corresponding Se XANES spectrum.

EXAFS Spectra

Se and Cu K-edge XAS spectra were collected from whole kidneys of rats fed 5 ppm Se diets. Se K-edge EXAFS spectra collected from a whole kidney and renal cortex sample were similar in appearance, although the lower noise level of the renal cortex spectrum indicated a higher Se concentration in this sample (Figure 8a). Cu K-edge EXAFS spectra were collected from the renal cortex and medulla (Figure 8b). The low concentration of Cu in the renal medulla is reflected in its noisy EXAFS spectrum, which makes analysis difficult and a direct comparison to the spectrum collected from the renal cortex unreliable.

Several fits to both the Se and Cu K-edge EXAFS spectra were attempted (Table 4) in order to test the hypothesis that Se-Cu bonding is responsible for the colocalisation of the two elements observed by XFM. Se K-edge EXAFS were initially fit with only Se scatterers (with a Se-Se bond length of about 2.36 Å, see Table 4, fit number 1), which generated good fits to spectra obtained from both the whole kidney and renal cortex. Figure 9a shows the calculated fit of Se scatterers only to the renal cortex spectrum. The addition of a S scatterer (with Se-S bond lengths of 2.21 and 2.17 Å in the whole and cortical kidney spectra, respectively) reduced the fit error, particularly to the renal cortex spectrum (Table 4, fit number 2). A similar improvement in the fits to the Se K-edge spectra was achieved with the addition of a Cu scatterer (with a Se-Cu bond length of 2.44 Å) instead of a S scatterer (Table 4, fit number 3), but the magnitude of ΔE_0 was higher than for fit number 2. Fitting Se, S and Cu scatterers to the whole kidney and renal cortex spectra (Table 4, fit number 4) did not improve on the fit consisting of the Se and S scatterers alone (fit number 2). In conclusion, the best fits to the Se K-edge EXAFS spectra include Se and S scatterers. Thus, analysis of the Se K-edge EXAFS spectra does not provide good evidence for the presence of a Se-Cu species in the tissues.

Analysis of Cu K-edge EXAFS spectra can provide further information on the presence of a Se-Cu species in tissues. Initially, N and S scatterers were fit to the Cu EXAFS spectra of both the cortex and medulla (Table 4 and Figure 9b). Due to the low concentrations of Cu in the medulla, the EXAFS spectrum was not amenable to further fitting attempts. A Se scatterer was added to fit the Cu EXAFS of the cortex, but this extra component lead only to a small reduction in fit error. There is also a discrepancy in the Cu-Se bond lengths determined from Se EXAFS (2.44 ± 1 Å) and Cu EXAFS (2.41 ± 1 Å) of the cortex, when the same bond lengths (within

1
2 error) would be expected if a Cu–Se bond was present. These observations support the fit
3 including only S and N scatterers to the Cu K-edge EXAFS spectra of the kidney tissue from
4 animal fed 5 ppm Se in the diet, but do not support the fit of a Se scatterer.
5
6
7

8
9 Thus, analysis of the Se and Cu EXAFS shows that the presence of a species containing a
10 Se–Cu bond is unlikely in the renal cortex of rats fed 5 ppm Se in the diet. Given the similarity
11 of the renal cortex and whole kidney Se EXAFS spectra, the result can be extrapolated to the
12 whole kidney. The most generous interpretation of these EXAFS results is that they could
13 indicate the presence of a Se–Cu species that is a minor component of the tissues compared to
14 the Se–Se species present.
15
16
17
18

19 20 *GPx1, but not SOD1, is increased in 5 ppm Se kidney tissues*

21
22 The response of two antioxidant enzymes to Se supplementation was examined at the gene and
23 protein level. Immunohistochemical staining revealed that SOD1 was ubiquitously distributed
24 across control kidneys and kidneys from animals fed 1 and 5 ppm Se in the diet (Figure 10a).
25 Consistent with our previous study,¹⁰ GPx1 showed a greater immune-positive response in the
26 kidney section from the animal fed 5 ppm Se in the diet (Figure 10b). In the corresponding
27 sections from the control and animal fed 1 ppm Se in the diet, GPx1 is distributed mostly in the
28 tubule epithelia (black arrows), but the distribution is extended into the tubular network in the
29 animal receiving 5 ppm Se in the diet, with some evidence of epithelial and endothelial staining
30 of the renal glomeruli (blue arrows).
31
32
33
34
35
36
37
38
39

40 Gene response studies support the immunohistochemical results. There was no difference in
41 SOD1 expression between the control, 1 ppm Se and 5 ppm Se tissues, but a 2.5-fold increase in
42 GPx expression was observed in the kidney tissue from the animal supplemented with 5 ppm Se
43 in the diet relative to the control (Figure 10c and d). It is likely that the increased GPx expression
44 accounts for some, but not all of the 10-fold increase in the Se concentration of the kidneys.
45
46
47
48
49

50 **Discussion**

51
52 Selenium metabolites exert the biological effects of dietary Se compounds. Thus, the study of Se
53 speciation *in vivo* is important in determining the efficacy of Se supplementation. In this study,
54 and for the first time, XFM and XAS techniques have been applied to investigate the distribution
55 and speciation of Se in the kidneys of rats fed a 5 ppm Se (as selenite) diet.
56
57
58
59
60

The most remarkable feature of this pilot study is the strongly correlated distribution of Se and Cu in the kidney of a rat fed a 5 ppm Se diet. Although imaging was performed on two

1
2 sections from a single tissue sample, the strength of the correlation, the increased Se levels
3 observed by ICP-MS and XAS studies of other samples, and the previously observed
4 colocalisation of Se and Cu in the cytosol of human lung cancer cells treated with selenite⁵ all
5 provide evidence for an intriguing relationship between exogenous Se and endogenous Cu. The
6 distribution was not observed in lung cancer cells treated with SeMet or MeSeCys,³ which
7 suggests that it is characteristic of selenite metabolism. Whether the metabolism occurs in the
8 local kidney region or some other organ or the blood prior to transport to the kidney is unclear.
9
10
11
12
13
14

15
16 An accumulation of both Se and Cu in the kidneys (measured by atomic absorption
17 spectroscopy and fluorimetry of digested tissues) has previously been observed in rats exposed
18 to 2, 4 or 8 ppm Se as selenite in drinking water *ad libitum* for 32 days. Rats exposed to 8 ppm
19 Se in drinking water had kidney Se concentrations (~18 ppm) approaching those observed in this
20 experiment (24 ± 3 ppm) and a 10-fold increase in kidney Cu concentration (increases in both Se
21 and Cu were also observed in the 4 ppm Se diets). In the study by Chen *et al.* there were some
22 signs of toxicity at all Se concentrations, but only at 8 ppm Se was severe reduction in food and
23 water intake observed.⁵⁰ In these experiments, the mean body mass of the rats fed the 5 ppm Se
24 diet (217 ± 8 g) was less than that of the rats on the control diet (230 ± 8 g), although the
25 difference was not significant ($P < 0.05$; two-tailed Student's *t*-test) and, by this measure, the rats
26 were not exhibiting signs of Se toxicity. More recently, drinking water containing 2.3 ppm Se as
27 selenite available *ad libitum* for 6 to 8 weeks resulted in no change in the body mass or relative
28 liver mass of rats compared to those fed control diets.⁵¹
29
30
31
32
33
34
35
36
37
38
39

40 Contrary to the report of Chen *et al.*,⁵⁰ ICP-MS results showed that there was no difference
41 in Cu concentrations between whole control kidneys and whole 5 ppm Se kidneys. Yet a 7-fold
42 increase in Cu was observed in the XFM image of the kidney section from the animal
43 supplemented with 5 ppm Se compared to the corresponding control section. The discord
44 between our ICP-MS and XFM measures of Cu levels may be due to biological variation, which
45 could also be true for our observation of Cu and Se colocalisation in the kidney. If the increase in
46 Cu observed in the sections imaged by XFM is due to the redistribution of Cu to the cortical
47 region of the tissue, ICP-MS of whole tissues would not be expected to indicate an increase in
48 Cu concentrations. Ideally, more samples for both ICP-MS and XFM analysis, and the separation
49 of ICP-MS tissues into cortical and medullary sections for analysis to better match the
50 observations from XFM, would resolve these issues. In the absence of more samples, we argue
51 that the evidence of a relationship, largely unexplored, between Se and Cu in selenite-treated
52 cells and rats that is already present in the literature,⁵⁰⁻⁵⁸ our own observations of a spatial
53 relationship between Se and Cu in selenite-treated cells⁵⁹ and the very strong correlation between
54
55
56
57
58
59
60

1
2 Se and Cu observed in the 5 ppm Se kidney sections themselves, makes this spatial relationship
3 worth reporting and investigating.
4
5

6
7 An antagonism between Se and Cu in biological systems is known in the literature,
8 although only between exogenously provided Se and Cu. For example, the concurrent
9 administration of Cu(II), as CuSO₄, to rats fed up to 20 ppm Se as selenite ameliorated the
10 effects of Se toxicity.⁵² The authors speculated that this effect could be due to binding of Cu to
11 proteins in place of Se metabolites, thereby limiting Se transport, or by the increased expression
12 of Cu-dependent enzymes such as SOD1 and cytochrome oxidase to protect against Se-induced
13 damage. In a similar experiment, co-administration of CuCl₂ and Na₂SeO₃ ameliorated the
14 toxicity of Se in rats fed with a diet containing up to 40 ppm selenite.⁵³ In that study it was
15 observed that as liver Se and Cu concentrations increased, the Cu:Se ratio decreased, leading the
16 authors to suggest that the formation of CuSe was rendering both Se and Cu less toxic. By
17 contrast, dietary Se supplementation (2 ppm Se as sodium selenite) did not prevent liver damage
18 in rats concurrently exposed to long term Cu(II) (as CuSO₄) supplementation.⁵⁴ The antagonism
19 of Se and Cu has been observed in primary human keratinocytes, where CuSO₄ protected the
20 cells against selenite toxicity.⁵⁵ Other studies suggest that an extracellular interaction of Cu and
21 Se is responsible for the protective effects of Cu against Se toxicity.^{56,57} In none of these studies
22 was the form of Se or Cu *in vivo* investigated. Recently, it was shown that a mixture of CuCl₂
23 and Na₂Se was non-toxic towards *Saccharomyces Cerevisiae* cells.⁵⁸ The authors showed that the
24 *in vitro* formation of CuSe rendered the otherwise toxic Cu²⁺ and Se²⁻ ions non-toxic.
25
26
27
28
29
30
31
32
33
34
35
36
37
38
39

40 The colocalisation of Se and Cu in the kidney tissues of the animal supplemented with
41 5ppm Se is much more exact than that recently observed in cells (which we attributed to Cu-Se
42 bonding and the upregulation of SOD1⁵⁹), and is tempting to ascribe to the aforementioned
43 antagonism between the two elements, possibly as a result of CuSe formation. However, this
44 possibility is not consistent with the weak evidence for Cu–Se bonding in the same kidney
45 tissues as judged by EXAFS and XANES spectra. The fitting of a linear combination of model
46 compounds to the Se K-edge XANES spectra produced the dubious result of high levels of CuSe
47 in all tissues, which was emphasized by the lack of evidence from EXAFS spectra for high levels
48 of Cu–Se bonding. This result may indicate the absence of an important Se model compound
49 from our library despite our efforts to cover a broad range of coordination environments (Figure
50 5). Nonetheless, the XANES fitting highlighted differences between the kidney spectra obtained
51 from control and animals supplemented with 1 or 5 ppm Se. The control and 1 ppm Se spectra
52 were fit with more C-bound (likely protein-bound) and S–Se–S species than the 5 ppm Se
53 spectra. Both EXAFS and XANES spectra collected from the 5 ppm Se kidney indicate the
54
55
56
57
58
59
60

1
2 presence of Se-Se species, which have previously been observed in human lung cancer cells
3 treated with high concentrations of selenite.⁵ Species containing Se–Se bonds include elemental
4 Se (which was fit to the XANES spectra), that is hypothesised to form from the oxidation of
5 HSe⁻,⁵⁸ and diselenide species, the presence of which could indicate an altered redox state.
6
7
8
9

10 Good fits to the Se EXAFS spectra were achieved with Se and S scatterers and good fits to
11 the Cu EXAFS spectra were achieved with S and N scatterers – the addition of Cu scatterers to
12 these fits garnered only slight improvements. Therefore, the strong colocalisation of Se and Cu
13 must be the result of another phenomenon. Increased SOD1 levels as a response to superoxide
14 production by metabolites of selenite explained, at least in part, both the increased Cu
15 concentrations and their colocalisation with Se in selenite-treated human lung cancer cells.⁵⁹
16 However, these experiments show that SOD1 is an unlikely source of increased Cu due to the
17 unchanged expression of SOD1 in the tissues. Its ubiquitous distribution in control and 5 ppm Se
18 kidneys is unlike the distribution of the Cu species colocalised with Se. In contrast, significantly
19 increased GPx1 expression appears to account for some of the increased Se concentration in the
20 kidneys, whereas in cells GPx1 showed a non-significant increase. Thus, the colocalisation of Se
21 and Cu in selenite-treated cells and in the kidneys of rats fed high Se diets appear to have
22 different origins. Selenite is rapidly metabolised by red blood cells⁶⁰ and therefore reaches the
23 kidneys in a different form to which it is administered, in contrast to the direct application of
24 selenite to cells *in vitro*. The unknown form(s) of Se entering the kidney versus the selenite
25 entering cells *in vitro* may be responsible for the different origins of the Se and Cu colocalisation
26 in these two model systems. Further research is required to determine if the accumulation of Cu
27 with Se is associated with protection against selenite-induced toxicity or if the biological activity
28 of Se is associated with a Cu specie(s).
29
30
31
32
33
34
35
36
37
38
39
40
41
42
43
44

45 SOD1 and direct bonding between Se and Cu are not likely to be significant contributors to
46 the colocalisation of Cu and Se in the renal sections, but the possibility that other proteins are
47 involved remains. Metallothioneins, which can bind Cu when it is present in excess and
48 participates in the detoxification of heavy metals,⁶¹ may be involved: selenolates are known to
49 form selenenylsulfide bonds at the metal-binding sites of metallothioneins *in vitro*.⁶²⁻⁶⁴ Further
50 investigation is required to determine the origin of the colocalisation of Cu and Se. Whether the
51 redistribution or accumulation of endogenous Cu to regions of high Se concentration in the
52 kidneys is a protective mechanism against selenite toxicity (similar to the as yet unknown
53 mechanism by which exogenous Cu protects against selenite toxicity *in vivo*), or, conversely,
54 contributes to the toxicity of selenite and its metabolites, remains to be determined.
55
56
57
58
59
60

1
2
3
4
5
6
7
8
9
10
11
12
13
14
15
16
17
18
19
20
21
22
23
24
25
26
27
28
29
30
31
32
33
34
35
36
37
38
39
40
41
42
43
44
45
46
47
48
49
50
51
52
53
54
55
56
57
58
59
60

This study does not provide a complete understanding of the origin or the nature of the accumulation of Cu and Se in the kidney. However, it does demonstrate the abilities of XFM and XAS techniques to reveal and to probe the relationships between Se and metals, in this case Cu, *in vivo*. The same techniques could be employed to determine whether the formation of Cu–Se moiety is indeed responsible for the antagonism observed when animals and cells are exposed to diets high in both Se and Cu. Refinement of the experiment described herein – such as more careful selection of tissue regions for imaging, spectroscopy and ICP-MS – in addition to upcoming developments at XFM beamlines that will allow imaging of frozen, hydrated tissue sections will make future experiments even more fruitful.

Acknowledgements

Graham N. George (University of Saskatchewan) provided Se K-edge X-ray absorption spectra of model Se compounds (except MeSeCys and GPx) and some model Cu compounds. Ninian Blackburn provided spectra of hCCS245Sec and Enzo Lombi also provided some model Cu compounds. Claire Wright (CSIRO Land and Water) performed microwave assisted digestion and ICP-MS measurements of kidney tissues. Use of the Advanced Photon Source at Argonne National Laboratory was supported by the U.S. Department of Energy, Office of Science, Office of Basic Energy Sciences, under Contract No. DE-AC02-06CH11357. Part of this research was undertaken at the X-ray Fluorescence Microprobe beamline at the Australian Synchrotron, Victoria, Australia. Portions of this research were carried out at the Stanford Synchrotron Radiation Lightsource, a Directorate of SLAC National Accelerator Laboratory and an Office of Science User Facility operated for the U.S. Department of Energy Office of Science by Stanford University. The SSRL Structural Molecular Biology Program is supported by the DOE Office of Biological and Environmental Research, and by the National Institutes of Health, National Center for Research Resources, Biomedical Technology Program (P41RR001209). We acknowledge travel funding provided by the International Synchrotron Access Program (ISAP) managed by the Australian Synchrotron and funded by the Australian Government, research funding from the Australian Research Council (DP0985807 to HHH) and the Australian Synchrotron Postgraduate Award (CMW).

References

1. C. B'Hymer and J. A. Caruso, *J. Chromatogr., A*, 2006, **1114**, 1–20.
2. M. A. Reeves and P. R. Hoffmann, *Cell. Mol. Life Sci.*, 2009, **66**, 2457–2478.
3. C. M. Weekley, J. B. Aitken, S. Vogt, L. A. Finney, D. J. Paterson, M. D. de Jonge, D. L. Howard, I. F. Musgrave, and H. H. Harris, *Biochemistry*, 2011, **50**, 1641–1650.
4. A. J. Duffield-Lillico, M. E. Reid, B. W. Turnbull, G. F. Combs Jr, E. H. Slate, L. A. Fischbach, J. R. Marshall, and L. C. Clark, *Cancer Epidemiol. Biomark. Prev.*, 2002, **11**, 630–639.
5. C. M. Weekley, J. B. Aitken, S. Vogt, L. A. Finney, D. J. Paterson, M. D. de Jonge, D. L. Howard, P. K. Witting, I. F. Musgrave, and H. H. Harris, *J. Am. Chem. Soc.*, 2011, **133**, 18272–18279.
6. C. M. Weekley, J. B. Aitken, I. F. Musgrave, and H. H. Harris, *Biochemistry*, 2012, **51**, 736–738.
7. C. M. Weekley, J. Aitken, L. A. Finney, S. Vogt, P. Witting, and H. Harris, *Nutrients*, 2013, **5**, 1734–1756.
8. S. Misra, D. Peak, N. Chen, C. Hamilton, and S. Niyogi, *Comp. Biochem. Phys. C*, 2012, **155**, 560–565.
9. S. J. Fairweather-Tait, Y. Bao, M. R. Broadley, R. Collings, D. Ford, J. E. Hesketh, and R. Hurst, *Antioxid. Redox Signal.*, 2011, **14**, 1337–1383.
10. A. Shanu, L. Groebler, H. B. Kim, S. Wood, C. M. Weekley, J. B. Aitken, H. H. Harris, and P. K. Witting, *Antioxid. Redox Signal.*, 2013, **18**, 756–769.
11. G. Dennert, M. Zwahlen, M. Brinkman, M. Vinceti, M. P. A. Zeegers, and M. Horneber, *Cochrane Database Syst. Rev.*, 2012, CD005195.
12. G. Flores-Mateo, A. Navas-Acien, R. Pastor-Barriuso, and E. Guallar, *Am. J. Clin. Nutr.*, 2006, **84**, 762–773.
13. S. Kehr, M. Malinouski, L. A. Finney, S. Vogt, V. M. Labunskyy, M. V. Kasaikina, B. A. Carlson, Y. Zhou, D. L. Hatfield, and V. N. Gladyshev, *J. Mol. Biol.*, 2009, **389**, 808–818.
14. S. Stranges, A. Navas-Acien, M. P. Rayman, and E. Guallar, *Nutr. Metab. Cardiovas. Dis.*, 2010, **20**, 754–760.
15. M. Malinouski, S. Kehr, L. A. Finney, S. Vogt, B. A. Carlson, J. Seravalli, R. Jin, D. E. Handy, T. J. Park, J. Loscalzo, D. L. Hatfield, and V. N. Gladyshev, *Antioxid. Redox Signal.*, 2012, **16**, 185–192.
16. M. P. Rayman, H. G. Infante, and M. Sargent, *Br. J. Nutr.*, 2008, **100**, 238–253.
17. H. B. Kim, A. Shanu, S. Wood, S. N. Parry, M. Collet, A. McMahon, and P. K. Witting, *Free Radic. Res.*, 2011, **45**, 1000–1012.
18. S. M. Lippman, E. A. Klein, P. J. Goodman, M. S. Lucia, I. M. Thompson, L. G. Ford, H. L. Parnes, L. M. Minasian, J. M. Gaziano, J. A. Hartline, J. K. Parsons, J. D. Bearden, E. D. Crawford, G. E. Goodman, J. Claudio, E. Winquist, E. D. Cook, D. D. Karp, P. Walther, M. M. Lieber, A. R. Kristal, A. K. Darke, K. B. Arnold, P. A. Ganz, R. M. Santella, D. Albanes, P. R. Taylor, J. L. Probstfield, T. J. Jagpal, J. J. Crowley, F. L. Meyskens, L. H. Baker, and C. A. Coltman, *JAMA*, 2009, **301**, 39–51.
19. D. L. Hatfield and V. N. Gladyshev, *Mol. Interv.*, 2009, **9**, 18–21.
20. C. M. Weekley and H. H. Harris, *Chem. Soc. Rev.*, 2013, **42**, 8870–8894.
21. E. A. Carter, B. S. Rayner, A. I. McLeod, L. E. Wu, C. P. Marshall, A. Levina, J. B. Aitken, P. K. Witting, B. Lai, Z. Cai, S. Vogt, Y.-C. Lee, C.-I. Chen, M. J. Tobin, H. H. Harris, and P. A. Lay, *Mol. Biosyst.*, 2010, **6**, 1316–1322.
22. N. Alwahaibi, J. Mohamed, and A. Alhamadani, *J. Trace Elem. Med. Biol.*, 2010, **24**, 119–123.
23. S. Tanguy, S. Morel, C. Berthonneche, M.-C. Toufektsian, M. de Lorgeril, V. Ducros, A. Tosaki, J. de Leiris, and F. Boucher, *Antioxid. Redox Signal.*, 2004, **6**, 792–796.
24. J. van Eersel, Y. D. Ke, X. Liu, F. Delerue, J. J. Kril, J. Götz, and L. M. Ittner, *Proc. Natl.*

- 1
2
3
4
5
6
7
8
9
10
11
12
13
14
15
16
17
18
19
20
21
22
23
24
25
26
27
28
29
30
31
32
33
34
35
36
37
38
39
40
41
42
43
44
45
46
47
48
49
50
51
52
53
54
55
56
57
58
59
60
- Acad. Sci. U.S.A.*, 2010, **107**, 13888–13893.
25. S. Vogt, *J. Phys. IV*, 2003, **104**, 635–638.
26. H. Shen, C. Yang, and C. Ong, *Int. J. Cancer*, 1999, **81**, 820–828.
27. T.-S. Kim, B. Y. Yun, and I. Y. Kim, *Biochem. Pharmacol.*, 2003, **66**, 2301–2311.
28. Y. Chen, E. McMillan-Ward, J. Kong, S. J. Israels, and S. B. Gibson, *J. Cell Sci.*, 2007, **120**, 4155–4166.
29. M. Wallenberg, E. Olm, C. Hebert, M. Björnstedt, and A. P. Fernandes, *Biochem. J.*, 2010, **429**, 85–93.
30. R. Kirkham, P. A. Dunn, A. J. Kuczewski, D. P. Siddons, R. Dodanwela, G. F. Moorhead, C. G. Ryan, G. de Geronimo, R. Beuttenmuller, D. Pinelli, M. Pfeffer, P. Davey, M. Jensen, D. J. Paterson, M. D. de Jonge, D. L. Howard, M. Kusel, J. McKinlay, R. Garrett, I. Gentle, K. Nugent, and S. Wilkins, *AIP*, vol. 1234, pp. 240–243.
31. M. Björnstedt, S. Kumar, and A. Holmgren, *J. Biol. Chem.*, 1992, **267**, 8030–8034.
32. S. Kumar, M. Björnstedt, and A. Holmgren, *Eur. J. Biochem.*, 1992, **207**, 435–439.
33. M. Björnstedt, M. Hamberg, S. Kumar, J. Xue, and A. Holmgren, *J. Biol. Chem.*, 1995, **270**, 11761–11764.
34. M. Pop, S. R. Davidson, M. Gertner, M. A. Jewett, M. D. Sherar, and M. C. Kolios, eds. F. Bello and S. Cotin, Springer, 2010, pp. 119–129.
35. K. T. Suzuki, Y. Ohta, and N. Suzuki, *Toxicol. Appl. Pharmacol.*, 2006, **217**, 51–62.
36. Y. Ogra, K. Ishiwata, H. Takayama, N. Aimi, and K. T. Suzuki, *J. Chromatogr., B*, 2002, **767**, 301–312.
37. Y. Kobayashi, Y. Ogra, K. Ishiwata, H. Takayama, N. Aimi, and K. T. Suzuki, *Proc. Natl. Acad. Sci. U.S.A.*, 2002, **99**, 15932–15936.
38. M. Lee, M. C. Rosario, H. H. Harris, R. E. Blankenship, J. M. Guss, and H. C. Freeman, *J. Biol. Inorg. Chem.*, 2009, **14**, 329–345.
39. Z. Veres, L. Tsai, T. D. Scholz, M. Politino, R. S. Balaban, and T. C. Stadtman, *Proc. Natl. Acad. Sci. U.S.A.*, 1992, **89**, 2975–2979.
40. R. S. Glass, W. P. Singh, W. Jung, Z. Veres, T. D. Scholz, and T. C. Stadtman, *Biochemistry*, 1993, **32**, 12555–12559.
41. R. S. Glass, M. J. Berry, E. Block, H. T. Boakye, B. A. Carlson, J. Gailer, G. N. George, V. N. Gladyshev, D. L. Hatfield, N. E. Jacobsen, S. Johnson, C. L. Kahakachchi, R. Kamiński, S. A. Manley, H. Mix, I. J. Pickering, E. J. Prenner, K. Saira, A. Skowrońska, J. F. Tyson, P. C. Uden, Q. Wu, X.-M. Xu, R. Yamdagni, and Y. Zhang, *Phosphorus, Sulfur Silicon Relat. Elem.*, 2008, **183**, 924–930.
42. B. Gammelgaard, M. I. Jackson, and C. Gabel-Jensen, *Anal. Bioanal. Chem.*, 2011, **399**, 1743–1763.
43. Y. Shiobara, Y. Ogra, and K. T. Suzuki, *Life Sci.*, 2000, **67**, 3041–3049.
44. M. Beilstein and P. Whanger, *J. Inorg. Biochem.*, 1988, **33**, 31–46.
45. K. T. Suzuki, C. Doi, and N. Suzuki, *Toxicol. Appl. Pharmacol.*, 2006, **217**, 185–195.
46. C. Gabel-Jensen, S. A. Bak, F. R. Lauritsen, H. R. Hansen, L. Badolo, and B. Gammelgaard, *J. Anal. At. Spectrom.*, 2009, **24**, 949–952.
47. C. Gabel-Jensen, J. Odgaard, C. Skonberg, L. Badolo, and B. Gammelgaard, *J. Anal. At. Spectrom.*, 2009, **24**, 69–75.
48. C. Gabel-Jensen and B. Gammelgaard, *J. Anal. At. Spectrom.*, 2010, **25**, 414–418.
49. K. Lunøe, C. Gabel-Jensen, S. Stürup, L. Andresen, S. Skov, and B. Gammelgaard, *Metallomics*, 2011, **3**, 162–168.
50. S. Y. Chen, P. J. Collipp, and J. M. Hsu, *Biol. Trace Elem. Res.*, 1985, **7**, 169–179.
51. S. Erkhembayar, A. Mollbrink, M. Eriksson, E. H. Larsen, and L. C. Eriksson, *J. Trace Elem. Med. Biol.*, 2011, **25**, 254–259.
52. W. Kezhou, H. D. Stowe, A. M. House, K. Chou, and T. Thiel, *J. Anim. Sci.*, 1987, **64**, 1467–1475.
53. L. Tatum, P. Shankar, L. M. Boylan, and J. Spallholz, *Biol. Trace Elem. Res.*, 2000, **77**,

- 1
2 241–249.
3
4 54. E. M. Aburto, A. E. Cribb, and C. Fuentealba, *Am. J. Vet. Res.*, 2001, **62**, 1423–1427.
5 55. C. L. Shen, W. Song, and B. C. Pence, *Cancer Epidemiol. Biomark. Prev.*, 2001, **10**, 385–
6 390.
7 56. R. Davis, J. Spallholz, and B. Pence, *Nutr. Cancer*, 1998, **32**, 181–189.
8 57. H. Zeng and J. H. Botnen, *J. Nutr. Biochem.*, 2004, **15**, 179–184.
9 58. M. Dauplais, M. Lazard, S. Blanquet, and P. Plateau, *PLoS ONE*, 2013, **8**, e54353.
10 59. C. M. Weekley, G. Jeong, M. E. Tierney, F. Hossain, A. M. Maw, A. Shanu, H. H. Harris,
11 and P. K. Witting, *J. Biol. Inorg. Chem.*, 2014.
12 60. K. T. Suzuki and M. Itoh, *J. Chromatogr. B Biomed. Sci. Appl.*, 1997, **692**, 15–22.
13 61. B. Ruttkay-Nedecky, L. Nejdil, J. Gumulec, O. Zitka, M. Masarik, T. Eckschlager, M.
14 Stiborova, V. Adam, and R. Kizek, *IJMS*, 2013, **14**, 6044–6066.
15 62. C. Jacob, W. Maret, and B. L. Vallee, *Proc. Natl. Acad. Sci. U.S.A.*, 1998, **95**, 3489–3494.
16 63. C. Jacob, W. Maret, and B. L. Vallee, *Biochem. Biophys. Res. Commun.*, 1998, **248**, 569–
17 573.
18 64. Y. Chen and W. Maret, *Antioxid. Redox Signal.*, 2001, **3**, 651–656.
19 65. A. N. Barry and N. J. Blackburn, *Biochemistry*, 2008, **47**, 4916–4928.
20
21
22
23
24
25
26
27
28
29
30
31
32
33
34
35
36
37
38
39
40
41
42
43
44
45
46
47
48
49
50
51
52
53
54
55
56
57
58
59
60

Tables and Figures

Table 1. Cu, Zn and Se concentrations of kidneys from rats fed control, 1 ppm and 5 ppm Se diets, as determined by XFM. The sections from which these concentrations were determined are shown in Figure 1.

diet	Cu (ppm)	Zn (ppm)	Se (ppm)	Cu:Se ratio
control ($n = 1$)	2.0	6.5	0.34	5.9
1 ppm Se ($n = 1$)	1.7	5.7	0.41	4.1
5 ppm Se ($n = 1$)	14	26	10	1.4

Table 2. Cu, Zn and Se concentrations of kidneys from rats fed control, 1 ppm and 5 ppm Se diets, as determined by ICP-MS.^a

diet	Cu (ppm)	Zn (ppm)	Se (ppm)	Cu:Se ratio
control ($n = 5$) ^b	40(12)	99(29)	5(2)	8.0
1 ppm Se ($n = 3$) ^c	28(24)	66(41)	4(3)	6.3
5 ppm Se ($n = 2$) ^d	43(7)	51(8)	24(3)	1.8

^aData are presented as mean (standard deviation). ^bKidneys from 4 individuals. ^cKidneys from 3 individuals. ^dKidneys from two individuals.

Table 3. Percent Se species in kidneys of rats fed control, 1 ppm Se or 5 ppm Se diets, as estimated by a linear combination of model compound spectra.

sample	elemental Se	CuSe	GPx	GSSeSG	N_{tot}	residual ($\times 10^{-3}$)
control	-	46(2)	18(2)	35.4(7)	0.99	0.47
1 ppm	-	33(2)	36(2)	33.3(8)	1.02	0.49
5 ppm (whole)	13.1(8)	58.5(7)	9.4(6)	19(1)	1.00	0.052
5 ppm (cortex)	27.7(2)	72.4(3)	-	-	1.00	0.11

^aValues in parentheses are the estimated standard deviations derived from the diagonal elements of the covariance matrix and are a measure of precision. ^b N_{tot} is the sum of the fractions.

Table 4. Parameters fit to Se and Cu EXAFS spectra of kidneys from rats fed 5 ppm Se (as selenite) diets for 3 weeks.^a

tissue	fit number	bond	coordination number (<i>N</i>)	interatomic distance (<i>R</i>)	Debye-Waller factor (σ^2 , Å ²)	$-\Delta E_0$ (eV)	fit error
whole kidney	1	Se-Se	2	2.361(3)	0.0035(1)	10(1)	32%
	2	Se-Se	2	2.373(5)	0.0038(1)	6(2)	30%
		Se-S	1	2.21(2)	0.006(1)		
	3	Se-Se	2	2.354(3)	0.0041(3)	11(2)	29%
		Se-Cu	1	2.44(4)	0.008(1)		
	cortex	4	Se-Se	1.5	2.377(9)	0.0023(4)	4(2)
Se-Cu			1	2.52(3)	0.008(2)		
1		Se-Se	2	2.367(2)	0.00300(7)	8.2(7)	25%
		Se-Se	2.65	2.371(2)	0.00406(7)		
2	Se-S	0.35	2.17(1)	0.0034(9)	7.7(7)	17%	
	Se-Se	2	2.35(3)	0.0041(1)			
cortex	3	Se-Cu	1	2.44(1)	0.0041(5)	11(1)	16%
		Se-Se	1.5	2.361(6)	0.0023(3)		
	4	Se-Cu	1	2.48(2)	0.0044(7)	7(2)	16%
		Se-S	0.5	2.19(1)	0.004(2)		
	1	Cu-S	1.5	2.30(4)	0.0026(3)	8(1)	29.5
		Cu-N	1.5	2.13(2)	0.008(2)		
Cu-Se		0.25	2.41(1)	0.0011(7)			
2	Cu-S	1.85	2.29(1)	0.008(3)	8(1)	28%	
	Cu-N	1.9	2.15(2)	0.005(3)			
medulla	1	Cu-N	2	1.893(9)	0.0036(6)	22(2)	71%
		Cu-S	2	2.249(9)	0.0071(6)		

^aThe best fits to each tissue are highlighted in bold. The *k*-range was 1 – 14.2 Å⁻¹ for Se EXAFS and 1 – 12.8 Å⁻¹ for Cu EXAFS and a scale factor (S_0^2) of 0.9 was used for all fits. $\Delta E_0 = E_0 - 12658$ eV for Se EXAFS and $\Delta E_0 = E_0 - 8979$ eV for Cu EXAFS where E_0 is the threshold energy. Values in parentheses are the estimated standard deviation derived from the diagonal elements of the covariance matrix and are a measure of precision. The fit-error is defined as $[\sum k^6 (\chi_{\text{exp}} - \chi_{\text{calc}})^2 / \sum k^6 \chi_{\text{exp}}^2]^{1/2}$.

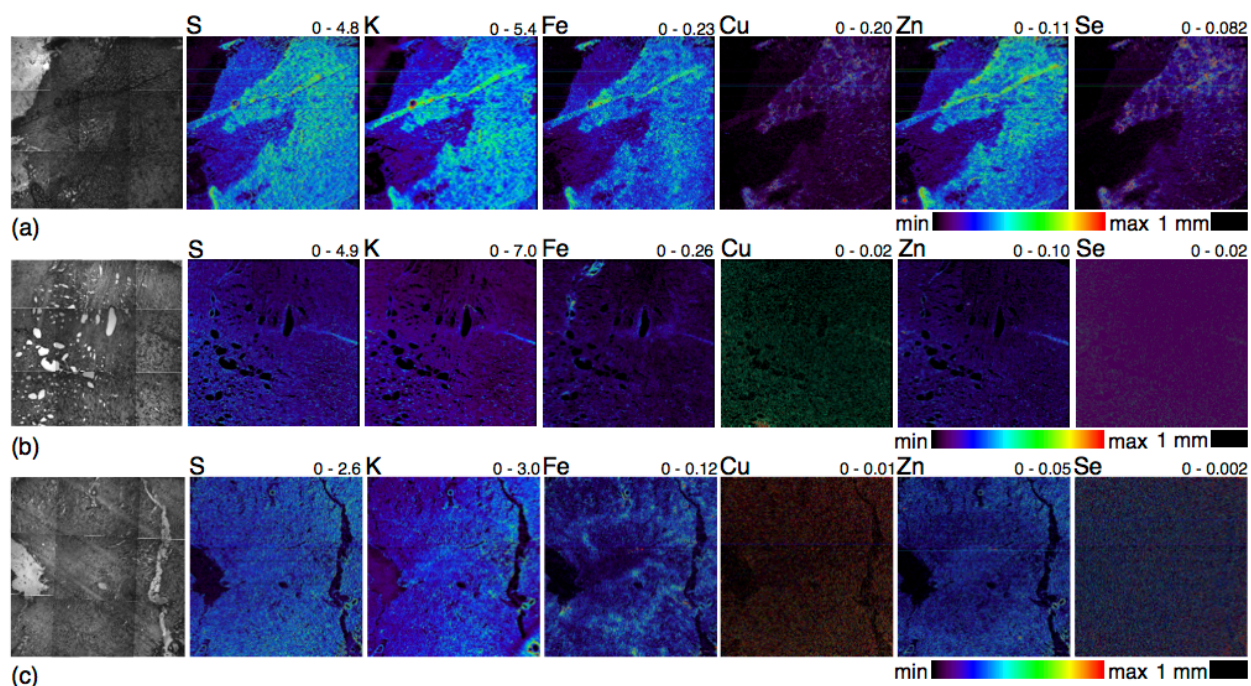


Figure 1. Visual (left) and XFM images of kidneys of rats fed a (a) 5 ppm Se or (b) 1 ppm Se (selenite) or (c) control diet for 3 weeks. Minimum and maximum concentrations ($\mu\text{g cm}^{-2}$) of each element are displayed at the top right of each elemental map and represent the range of the colour map for each image.

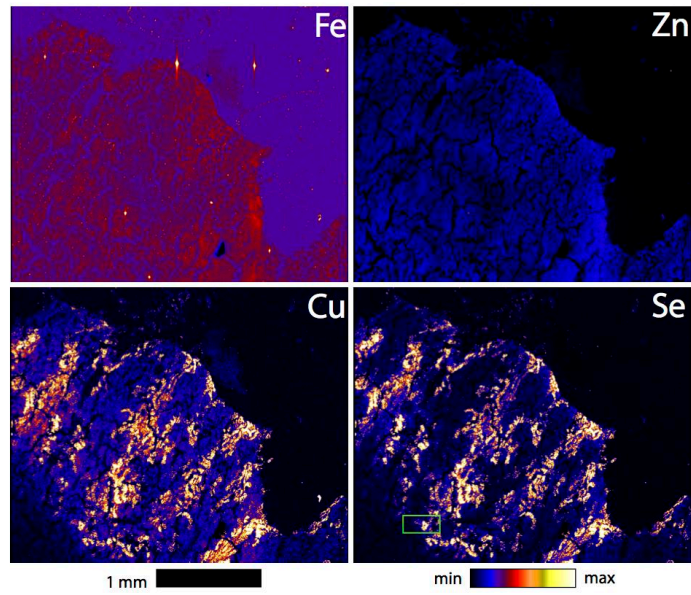


Figure 2. X-ray fluorescence microscope images of a kidney section ($30\ \mu\text{m}$ thick) from a rat fed a 5 ppm Se (as selenite) diet for 3 weeks.

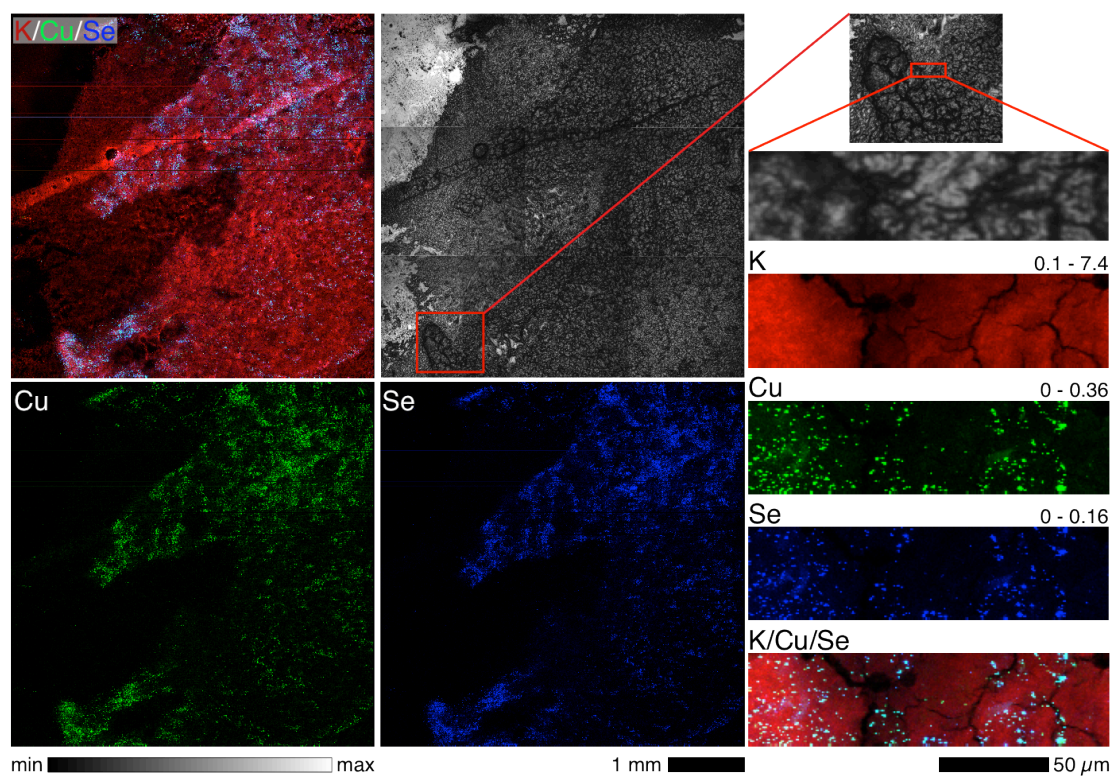


Figure 3. Colocalisation of Cu and Se in a kidney section of a rat fed a 5 ppm Se diet. The whole image is shown (left) along with a higher resolution image of a small region (right). The K, Cu and Se images are overlaid to show the coincidence of Se and Cu, which appears light blue. The range of the elemental area density ($\mu\text{g cm}^{-2}$) is given in the top right of the small maps.

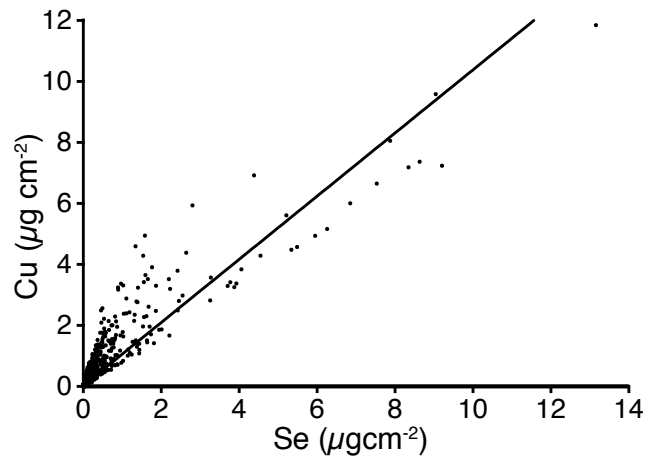


Figure 4. Linear regression of Cu concentration against Se concentration at each point in the small region shown in Figure 3 (~ 14000 points): slope = 1.036 ± 0.004 , $R^2 = 0.84$.

1
2
3
4
5
6
7
8
9
10
11
12
13
14
15
16
17
18
19
20
21
22
23
24
25
26
27
28
29
30
31
32
33
34
35
36
37
38
39
40
41
42
43
44
45
46
47
48
49
50
51
52
53
54
55
56
57
58
59
60

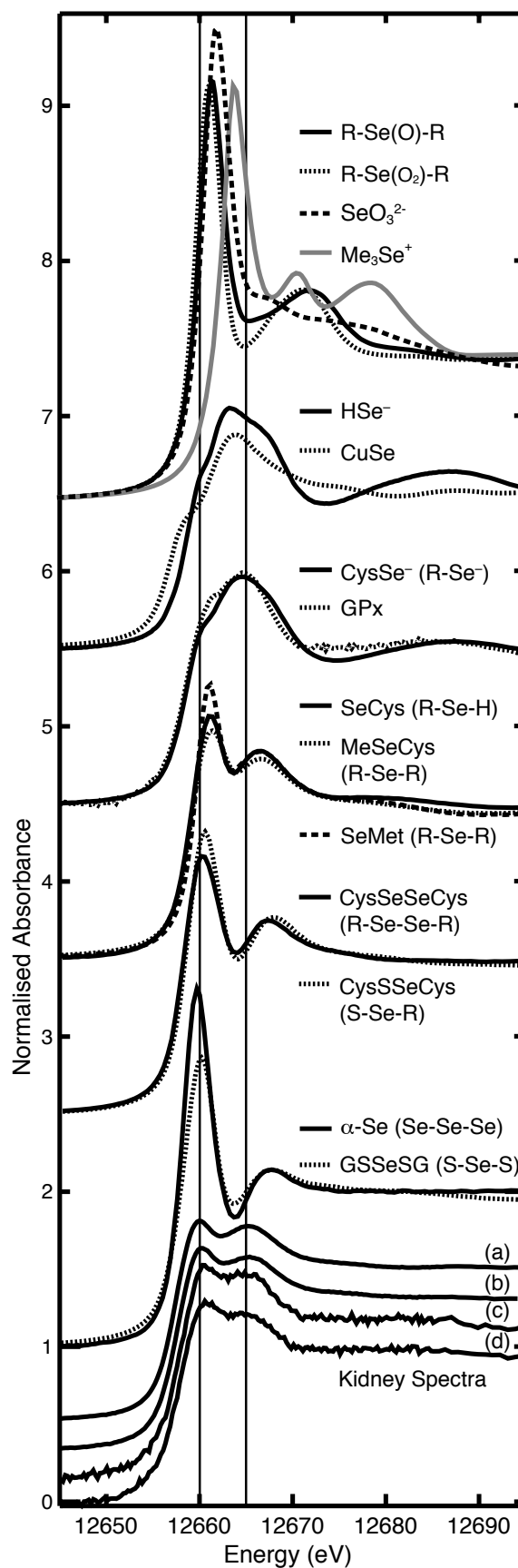


Figure 5. Se XANES of Se model compounds used in the fitting of kidney XANES spectra, which are also shown for comparison: (a) renal cortex and (b) whole kidney from rats fed a 5 ppm Se diet and kidneys from rats fed a (c) 1 ppm Se and (d) control diet. Dashed lines align with the absorption peaks in kidney spectrum (d).

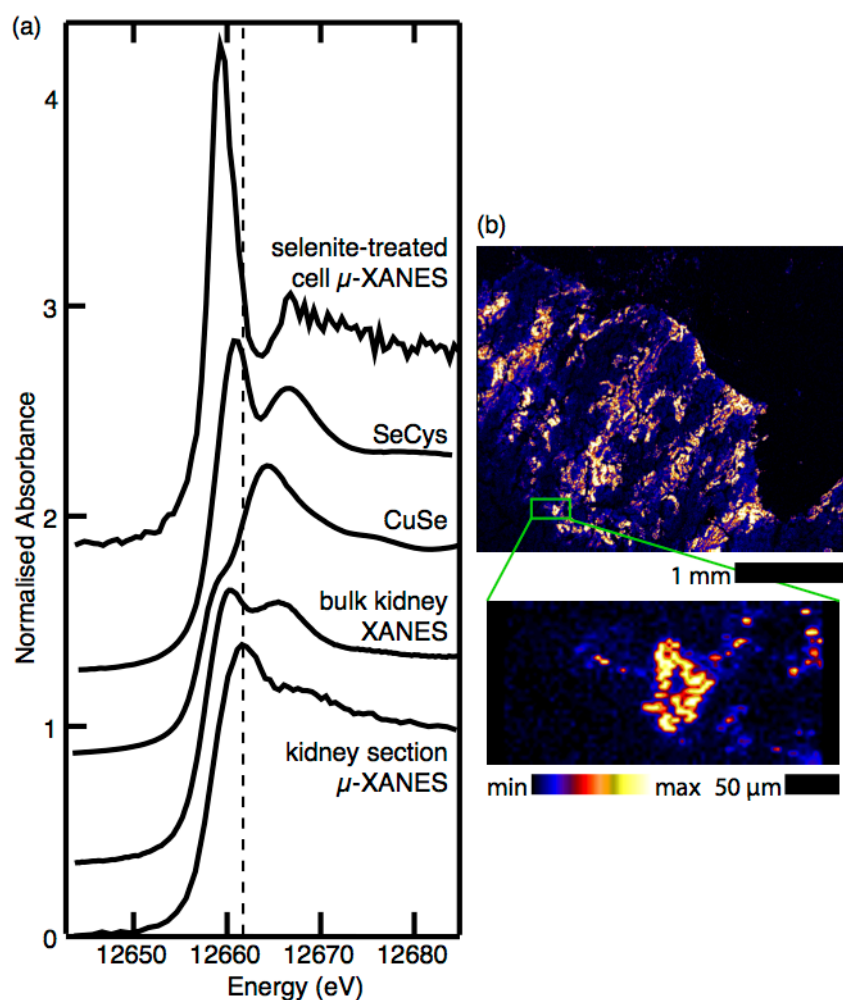


Figure 6. (a) Se μ -XANES spectrum extracted from (b) XFM images, collected at a number of different energies, of a small region of renal tissue section from a rat fed a 5 ppm Se diet. The kidney section μ -XANES spectrum is plotted with a bulk kidney XANES spectrum from a corresponding whole kidney, CuSe and SeCys model compound XANES spectra and the μ -XANES spectrum collected previously from human lung cancer cells treated with 5 μ M selenite.⁵

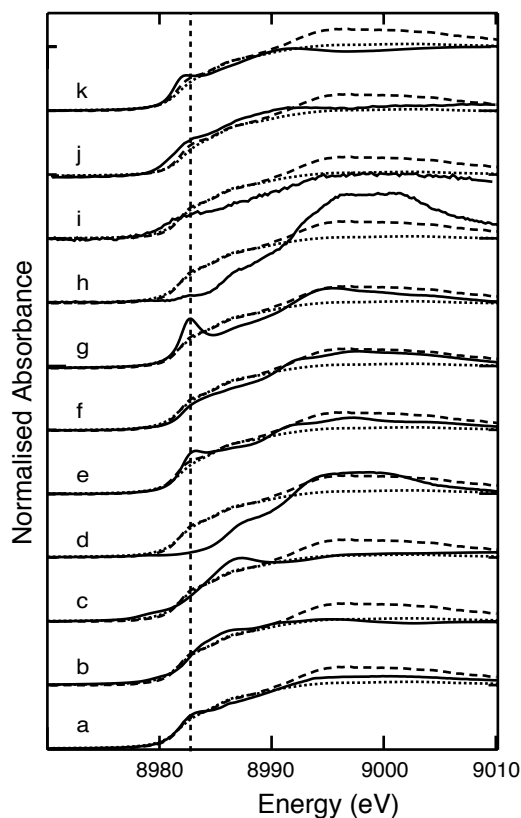


Figure 7. Cu K-edge XANES spectra of cortical (dotted) and medullary (dashed) regions of a kidney from a rat fed a 5 ppm Se diet for 3 weeks compared to: a spectrum of (a) A549 human lung cancer cells treated with 5 μ M selenite for 24 h and (b-j) Cu compound and Cu protein spectra (black). The Cu compound and protein spectra displayed are: (b) CuSe, (c) CuS, (d) Cu-histidine, (e) Cu(I)-auracyanin a (mixed Cu-S/Cu-N), (f) Cu(II)-auracyanin a (mixed Cu-S/Cu-N), (g) Cu(I)SOD, (h) Cu(II)SOD, (i) Cu,Zn-SOD, (j) Cu-metallothionein, (k) a selenocysteine variant of the human copper chaperone protein (hCCS245Sec) (Cu-Se).⁶⁵

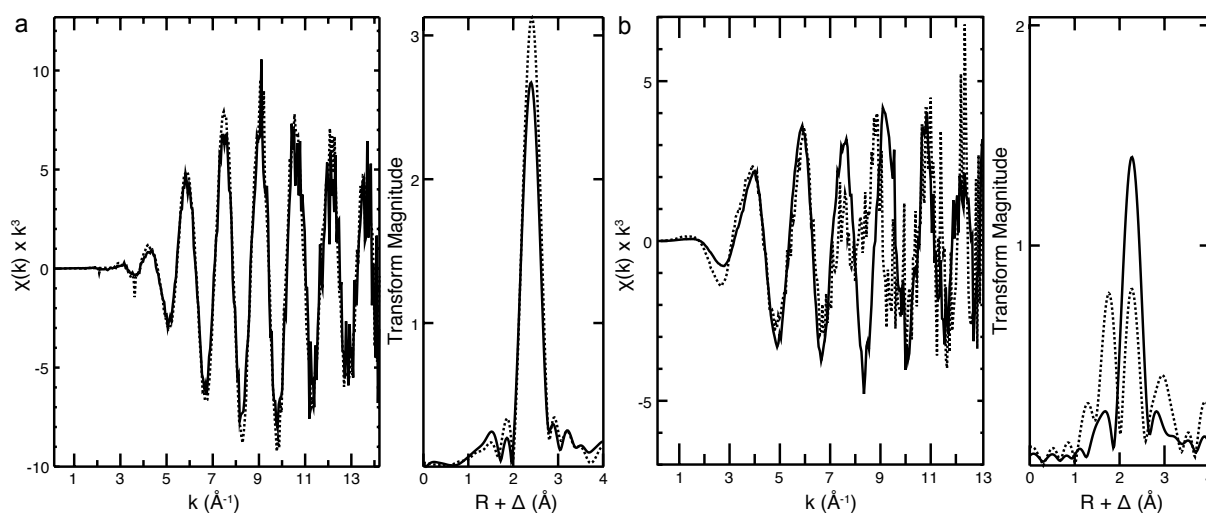


Figure 8. (a) Se K-edge EXAFS spectra (left) and the corresponding Fourier transforms (right) of whole kidney (solid line) and renal cortex (dotted line). (b) Cu K-edge EXAFS spectra (left) and the corresponding Fourier transforms (right) of renal cortex (solid line) and medulla (dotted line). Fit parameters are listed in Table 4.

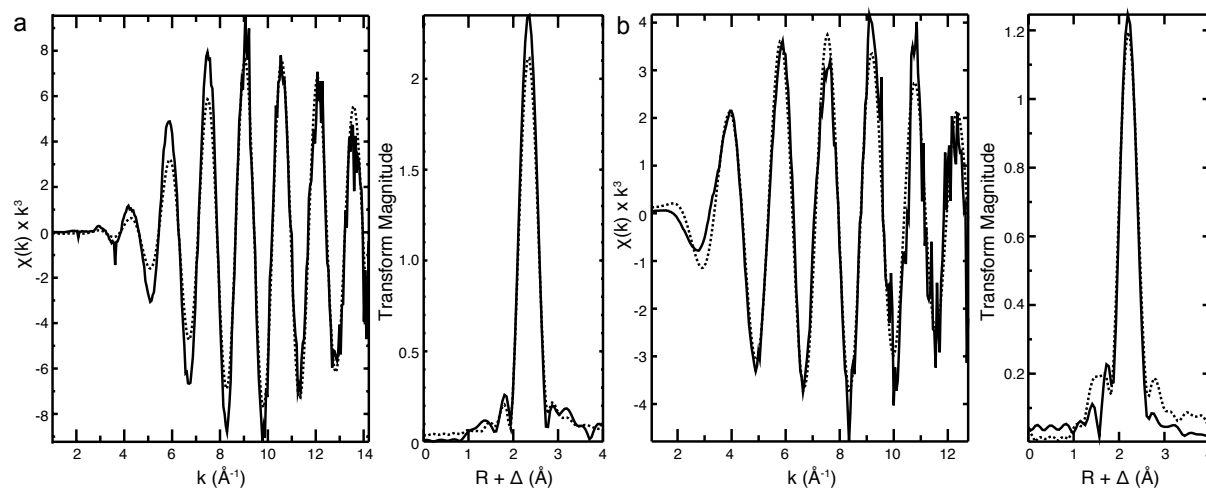


Figure 9. (a) Se K-edge EXAFS spectrum (left) and the corresponding Fourier Transform (right) of the renal cortex (solid line), with the calculated fit (dotted line) for 2 Se scatterers. (b) Cu K-edge EXAFS spectrum (left) and the corresponding Fourier Transform (right) of the renal cortex (solid line), with the calculated fit (dotted line) for 1.5 S and 1.5 N scatterers. Fit parameters are listed in Table 4.

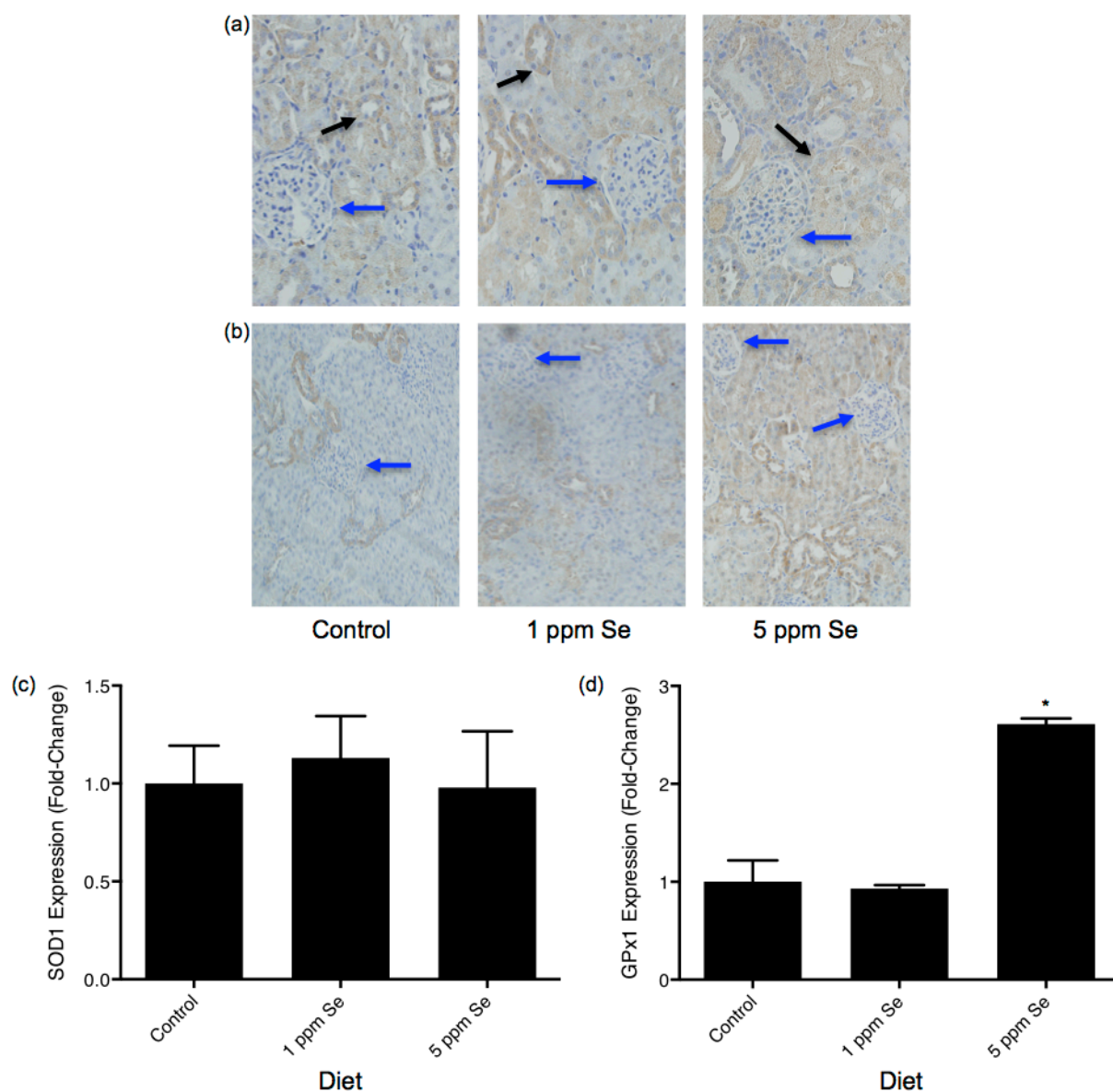
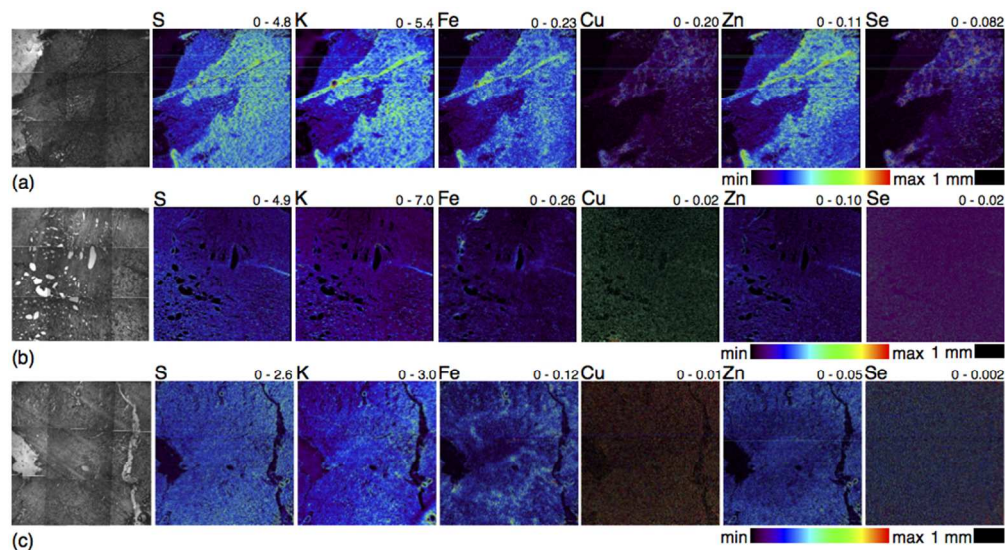
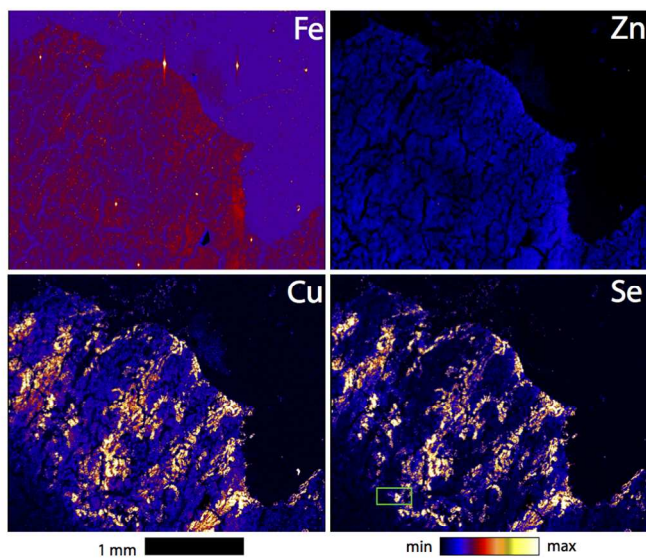


Figure 10. Distribution of immunoactive (a) SOD1 and (b) GPx1 in renal sections of rats fed control, 1 ppm Se and 5 ppm Se diets. Black arrows indicate immune-active staining (brown) in the epithelial cells lining the proximal tubules. Blue arrows indicate glomeruli (round features). Fold-change in (c) SOD1 and (d) GPx1 expression in kidneys from rats fed high Se diets compared to rats fed control diets. Data representing mean \pm SD; $n = 4$ independent experiments. *Different to the control; $P < 0.05$ as determined by two-tailed Student's t -test, assuming equal variance.

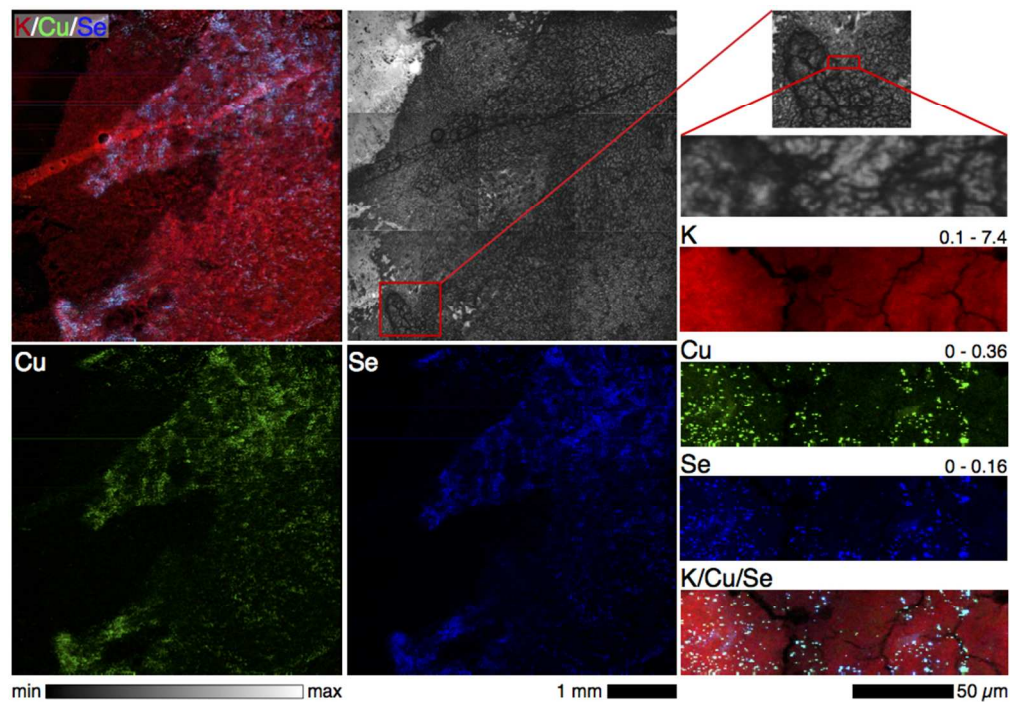


Visual (left) and XFM images of kidneys of rats fed a (a) 5 ppm Se or (b) 1 ppm Se (selenite) or (c) control diet for 3 weeks. Minimum and maximum concentrations ($\mu\text{g cm}^{-2}$) of each element are displayed at the top right of each elemental map and represent the range of the colour map for each image.
170x93mm (150 x 150 DPI)

1
2
3
4
5
6
7
8
9
10
11
12
13
14
15
16
17
18
19
20
21
22
23
24
25
26
27
28
29
30
31
32
33
34
35
36
37
38
39
40
41
42
43
44
45
46
47
48
49
50
51
52
53
54
55
56
57
58
59
60

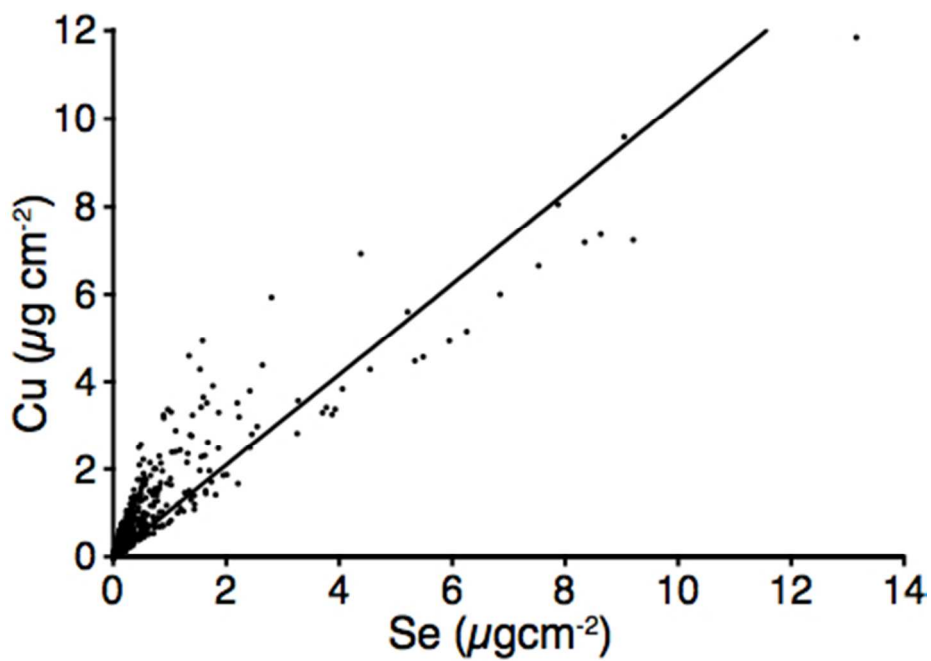


X-ray fluorescence microscope images of a kidney section (30 μm thick) from a rat fed a 5 ppm Se (as selenite) diet for 3 weeks.
209x296mm (150 x 150 DPI)

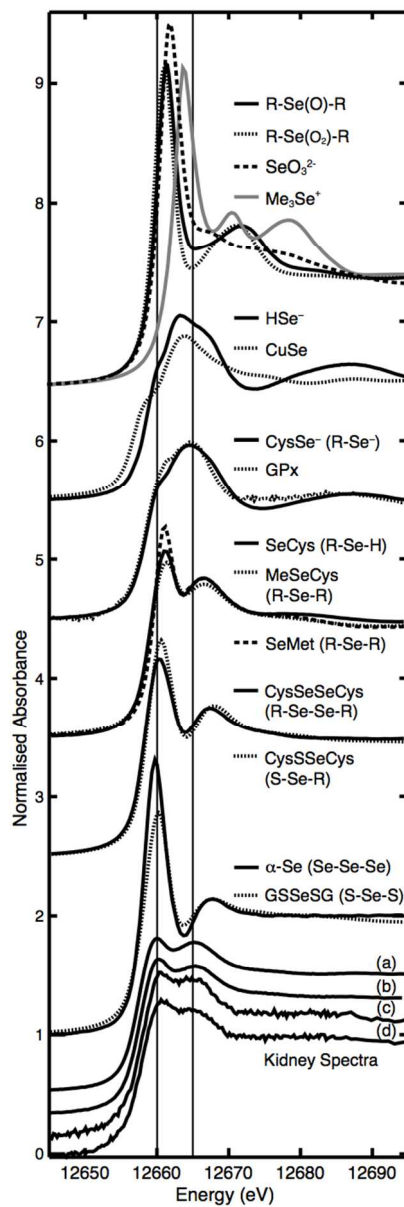


Colocalisation of Cu and Se in a kidney section of a rat fed a 5 ppm Se diet. The whole image is shown (left) along with a higher resolution image of a small region (right). The K, Cu and Se images are overlaid to show the coincidence of Se and Cu, which appears light blue. The range of the elemental area density ($\mu\text{g cm}^{-2}$) is

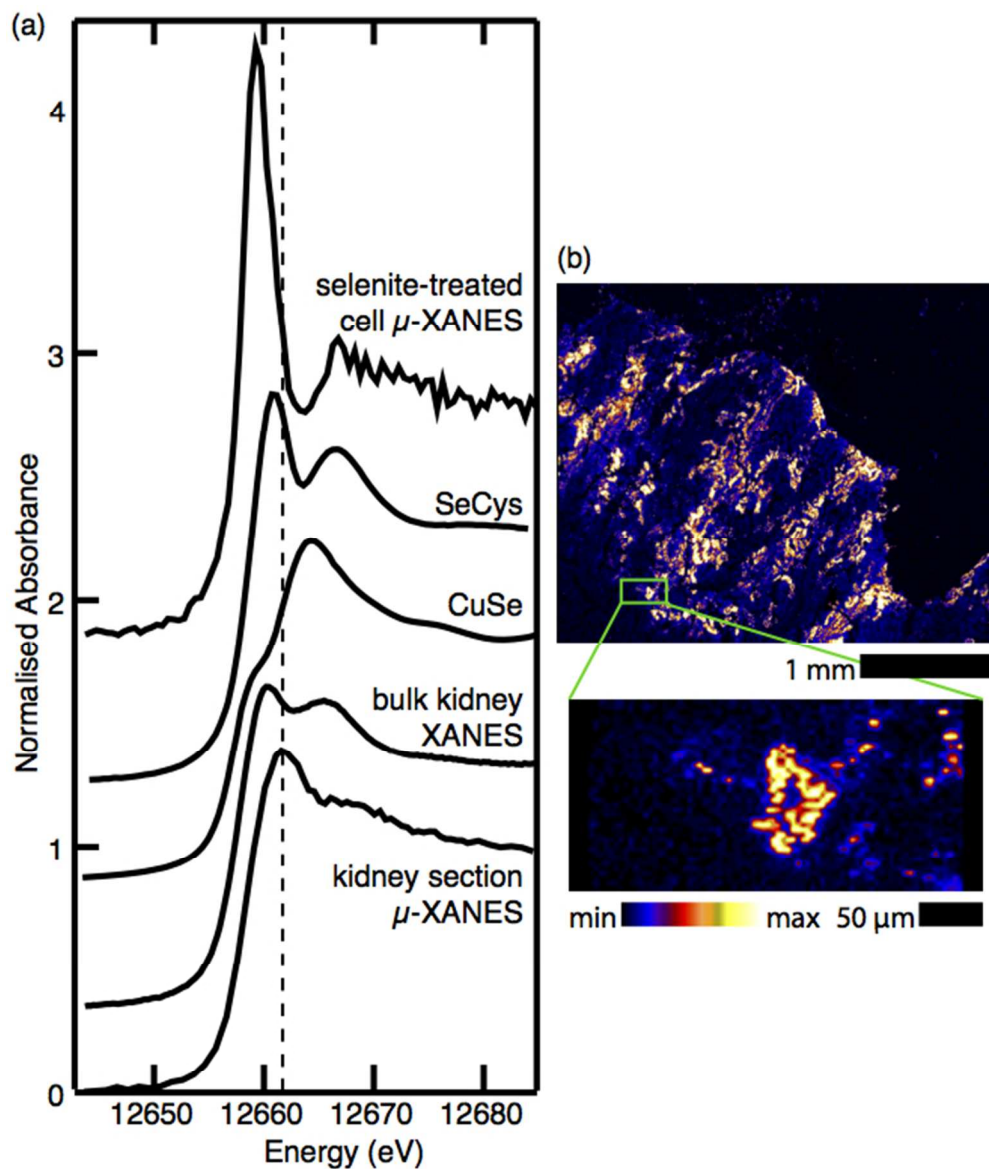
170x119mm (150 x 150 DPI)



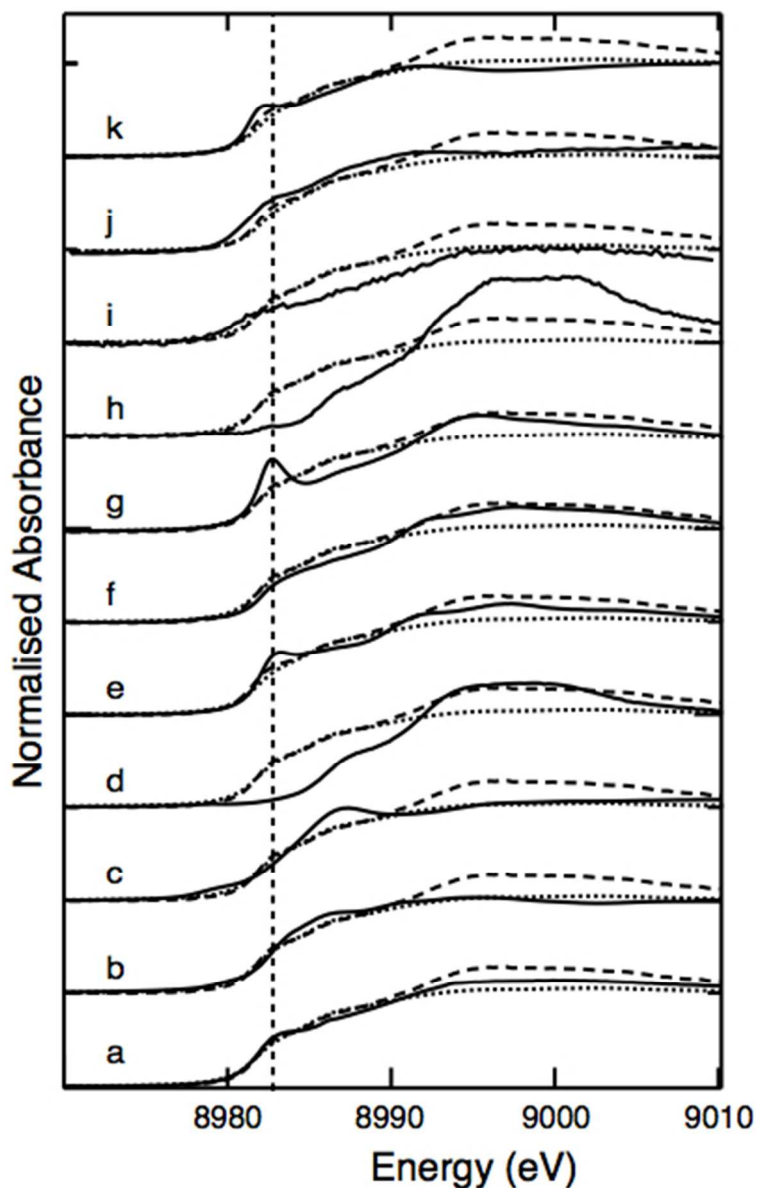
Linear regression of Cu concentration against Se concentration at each point in the small region shown in Figure 3 (~ 14000 points): slope = 1.036 ± 0.004 , $R^2 = 0.84$.
77x55mm (150 x 150 DPI)



Se XANES of Se model compounds used in the fitting of kidney XANES spectra, which are also shown for comparison: (a) renal cortex and (b) whole kidney from rats fed a 5 ppm Se diet and kidneys from rats fed a (c) 1 ppm Se and (d) control diet. Dashed lines align with the absorption peaks in kidney spectrum (d).
80x239mm (150 x 150 DPI)

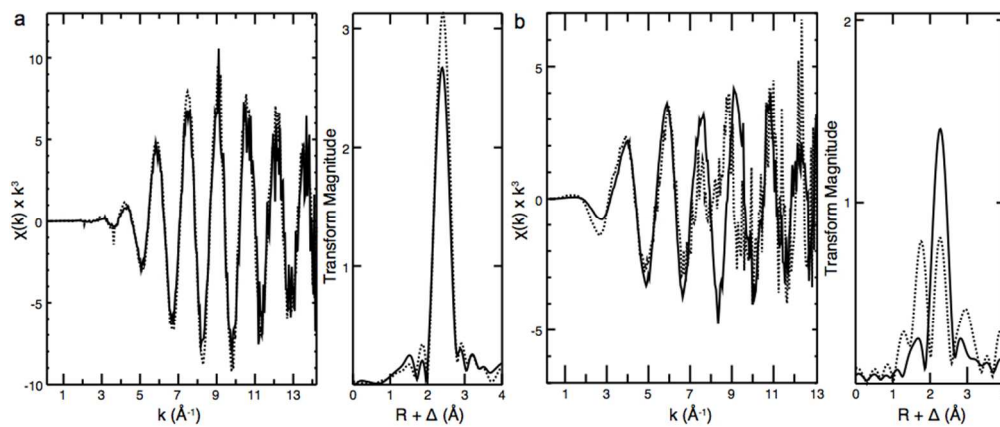


(a) Se μ -XANES spectrum extracted from (b) XFM images, collected at a number of different energies, of a small region of renal tissue section from a rat fed a 5 ppm Se diet. The kidney section μ -XANES spectrum is plotted with a bulk kidney XANES spectrum from a corresponding whole kidney, CuSe and SeCys model compound XANES spectra and the μ -XANES spectrum collected previously from human lung cancer cells treated with 5 μ M selenite.⁵
112x131mm (150 x 150 DPI)

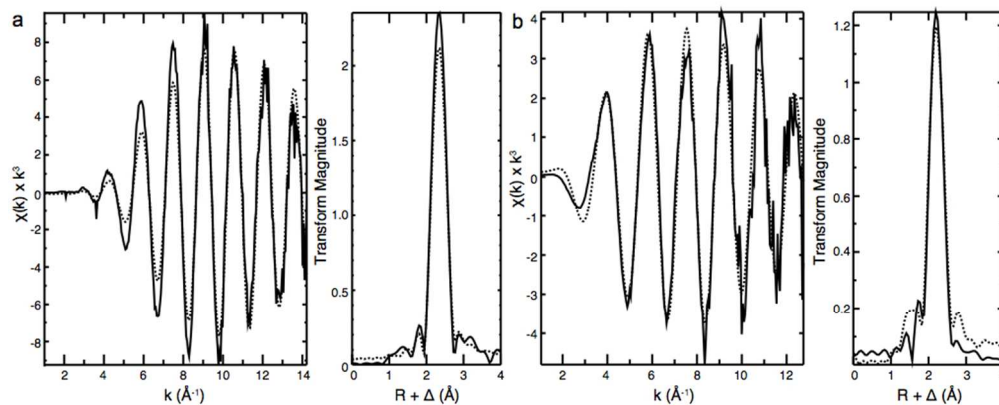


Cu K-edge XANES spectra of cortical (dotted) and medullary (dashed) regions of a kidney from a rat fed a 5 ppm Se diet for 3 weeks compared to: a spectrum of (a) A549 human lung cancer cells treated with 5 μ M selenite for 24 h and (b-j) Cu compound and Cu protein spectra (black). The Cu compound and protein spectra displayed are: (b) CuSe, (c) CuS, (d) Cu-histidine, (e) Cu(I)-auracyanin a (mixed Cu-S/Cu-N), (f) Cu(II)-auracyanin a (mixed Cu-S/Cu-N), (g) Cu(I)SOD, (h) Cu(II)SOD, (i) Cu,Zn-SOD, (j) Cu-metallothionein, (k) a selenocysteine variant of the human copper chaperone protein (hCCS245Sec) (Cu-Se).⁶⁵

83x108mm (150 x 150 DPI)



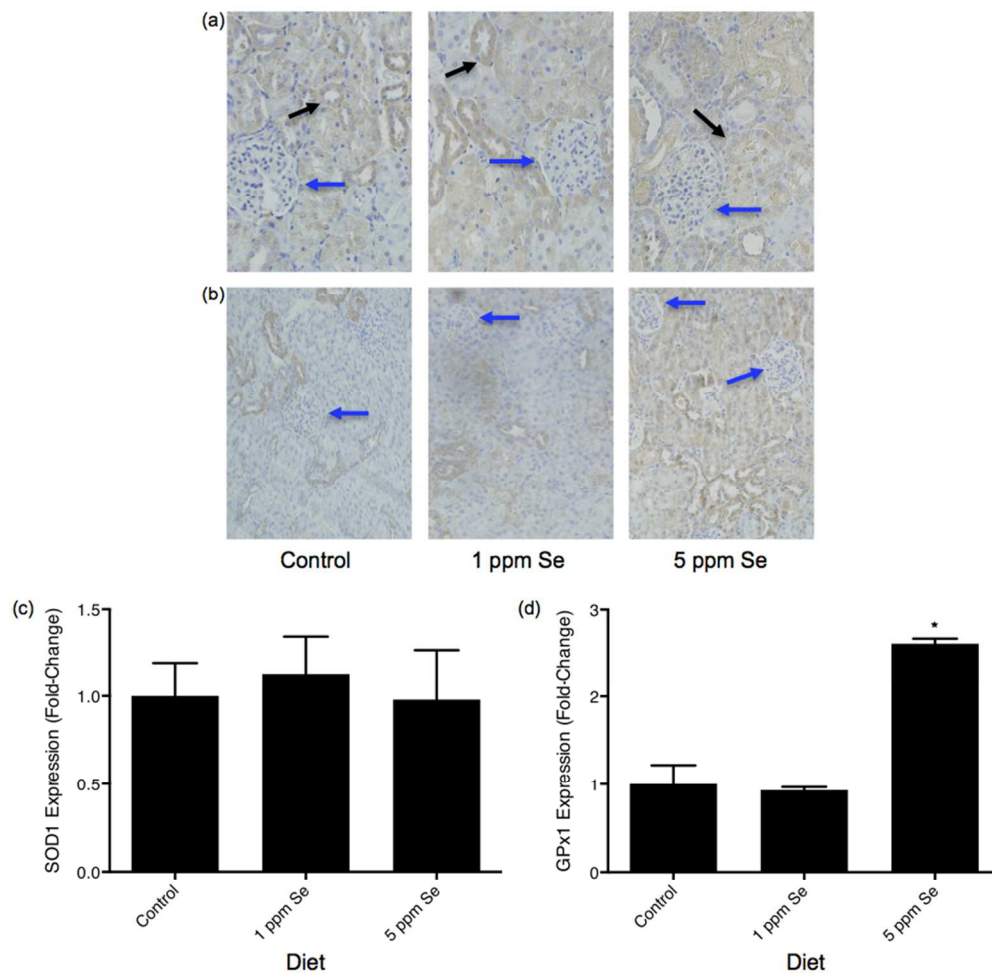
(a) Se K-edge EXAFS spectra (left) and the corresponding Fourier transforms (right) of whole kidney (solid line) and renal cortex (dotted line). (b) Cu K-edge EXAFS spectra (left) and the corresponding Fourier transforms (right) of renal cortex (solid line) and medulla (dotted line). Fit parameters are listed in Table 4. 172x71mm (150 x 150 DPI)



(a) Se K-edge EXAFS spectrum (left) and the corresponding Fourier Transform (right) of the renal cortex (solid line), with the calculated fit (dotted line) for 2 Se scatterers. (b) Cu K-edge EXAFS spectrum (left) and the corresponding Fourier Transform (right) of the renal cortex (solid line), with the calculated fit (dotted line) for 1.5 S and 1.5 N scatterers. Fit parameters are listed in Table 4.

172x71mm (150 x 150 DPI)

1
2
3
4
5
6
7
8
9
10
11
12
13
14
15
16
17
18
19
20
21
22
23
24
25
26
27
28
29
30
31
32
33
34
35
36
37
38
39
40
41
42
43
44
45
46
47
48
49
50
51
52
53
54
55
56
57
58
59
60



Distribution of immunoactive (a) SOD1 and (b) GPx1 in renal sections of rats fed control, 1 ppm Se and 5 ppm Se diets. Black arrows indicate immune-active staining (brown) in the epithelial cells lining the proximal tubules. Blue arrows indicate glomeruli (round features). Fold-change in (c) SOD1 and (d) GPx1 expression in kidneys from rats fed high Se diets compared to rats fed control diets. Data representing mean \pm SD; n = 4 independent experiments. *Different to the control; P < 0.05 as determined by two-tailed Student's t-test, assuming equal variance.
161x156mm (150 x 150 DPI)